Wave pattern induced by a localized obstacle in the flow of a one-dimensional polariton condensate

P.-É. Larré,[1] N. Pavloff,[1] and A. M. Kamchatnov[2]

[1]*Univ. Paris-Sud, CNRS, Laboratoire de Physique Théorique et Modèles Statistiques, UMR8626, F-91405 Orsay, France*

[2]*Institute of Spectroscopy, Russian Academy of Sciences, Troitsk, Moscow Region, 142190, Russia*

(Received 10 July 2012; revised manuscript received 19 September 2012; published 4 October 2012)

Motivated by recent experiments on generation of wave patterns by a polariton condensate incident on a localized obstacle, we study the characteristics of such flows under the condition that irreversible processes play a crucial role in the system. The dynamics of a nonresonantly pumped polariton condensate in a quasi-one-dimensional quantum wire is modeled by a Gross-Pitaevskii equation with additional phenomenological terms accounting for the dissipation and pumping processes. The response of the condensate flow to an external potential describing a localized obstacle is considered in the weak-perturbation limit and also in the nonlinear regime. The transition from a viscous drag to a regime of wave resistance is identified and studied in detail.

DOI: 10.1103/PhysRevB.86.165304 PACS number(s): 03.75.Kk, 71.36.+c

I. INTRODUCTION

The ability to move with respect to an obstacle without dissipating energy is one of the most intuitive and appealing definitions of superfluidity. This is the reason why the motion of quantum fluids with respect to obstacles has been used in several experiments aiming at revealing a superfluid behavior in different physical systems: ^{4}He (see, e.g., Refs. 1 and 2), ^{3}He (Ref. 3), ultracold atomic vapors,[4–8] and more recently polariton condensates.[9–13]

For a weakly perturbing impurity moving at constant velocity V in a conservative atomic Bose-Einstein condensed (BEC) system at zero temperature, the Landau criterion[14] predicts that there exists a critical velocity $V_{\rm crit}$ separating two different behaviors: (i) for $V < V_{\rm crit}$ no excitations are emitted away from the obstacle and, hence, there is no drag force; (ii) for $V > V_{\rm crit}$ a Cherenkov radiation of linear waves occurs; these waves carry momentum away from the impurity which is thus subject to a finite drag force. The first regime is superfluid and the second one is dissipative.[15]

In a pumped nonequilibrium polariton condensate, even when kinematically allowed, propagating disturbances are always damped due to the finite lifetime of the polaritons. As a result, the well-defined transition between superfluid and dissipative regimes transforms in these damped systems into a crossover characterized by different forms of wave patterns: localized for small enough flow velocity, oscillatory and extended for large enough flow velocity. The boundary between these two regimes is typically not abrupt: Just at the transition point the decay length of a propagating wave is less than its wavelength and this disturbance can hardly be distinguished from a localized perturbation. It might thus be difficult to separate a superfluid regime from a dissipative one by studying the wave pattern created by an obstacle. Nevertheless, the concept of superfluidity is often employed because it permits a simple qualitative discussion of the processes taking place in the flow of a polariton condensate.

In the present work we study in detail the wake of a polariton condensate past an obstacle and the associated drag force. We argue that, for low enough damping, the superfluid/dissipative transition is better understood in terms of a crossover of the force experienced by the obstacle from a viscous drag to wave resistance, in analogy to what is observed for capillary-gravity waves.

The paper is organized as follows. In Sec. II we present the phenomenological one-dimensional model we use and present our strategy for studying the specific features of typical flows. In Sec. III we set up a general perturbative analysis of the motion of the polariton gas past a weak obstacle and discuss the domain of validity of this approach. In Sec. IV we obtain nonperturbative results valid for a localized narrow impurity using several approximation schemes (the so-called hydraulic approximation in Sec. IV A and Whitham averaging method in Sec. IV B) and also numerical integration (Sec. IV C). Finally we present our conclusions in Sec. V. Some technical points are given in the appendices. In Appendix A we study the poles of the response function of the system and in Appendix B we present the perturbed Whitham theory we use in Sec. IV B of the main text.

II. THE MODEL

We study the flow of a polariton condensate past an obstacle disregarding possible effects of polarization of the light modes in the cavity. We consider a configuration in which excitons are confined in a one-dimensional quantum wire and, as a result, the polariton condensate is described by an order parameter $\psi(x,t)$ whose dynamics is modeled by a Gross-Pitaevskii equation of the form

$$i\hbar\,\psi_t = -\frac{\hbar^2}{2m}\,\psi_{xx} + (U_{\rm ext}(x,t) + \alpha\rho)\psi + i(\gamma - \Gamma\rho)\psi. \tag{1}$$

In Eq. (1) m is the polariton effective mass (in the parabolic dispersion approximation, valid at small momenta), $\rho(x,t) = |\psi(x,t)|^2$ is the polariton density, and $U_{\rm ext}(x,t)$ describes the potential of a localized obstacle, possibly in motion relative to the polariton gas. Interaction effects are described by an effective local repulsive term characterized by the nonlinear coupling constant $\alpha > 0$. There is a whole body of evidence showing that the overall effective interaction between polaritons is repulsive. Some of the most direct manifestations of this repulsion are the observed emission

blueshift[16–18] and the expulsion of the condensate from a pumping region.[19,20] Another consequence of repulsion, very important for the present study, is the absence of scattering from a defect—first observed in Refs. 9 and 10—and the related emission of nonlinear excitations[15] (solitons and vortices) whose generation is typically associated with a loss of superfluidity.[11–13,21]

Due to the finite lifetime of the polaritons, the system needs to be pumped. Following Refs. 22–26, we schematically describe this effect by the last term of Eq. (1): The term $\hbar\,\psi_t = \gamma\,\psi$ phenomenologically describes the combined effects of the pumping and decay processes.[27] For $\gamma > 0$ an overall gain leads, if not compensated, to an exponential increase of the density. This increase is counterbalanced by the term $\hbar\,\psi_t = -\Gamma\rho\,\psi$ (where $\Gamma > 0$) which accounts for a saturation of the gain at large density and allows one to reach a steady-state configuration—resulting from dynamical equilibrium between gain and losses—with a finite density $\rho_0 = \gamma/\Gamma$. Equation (1) corresponds to a situation where the pumping extends over all space. This models a system where an obstacle is present within a large reservoir, and simplifies the theoretical treatment because the stationary density in the absence of external potential is constant. Results where the obstacle is present outside of the pumping region will be presented in a forthcoming publication.[28]

Localized structural defects are naturally present in many samples; they can also be artificially created by means of lithographic techniques or by a continuous-wave laser. If an obstacle is introduced into the condensate, the state with uniform density ρ_0 is disturbed. We suppose that the obstacle is described by a potential $U_{\rm ext}(x,t)$ with a finite spatial extension [verifying $U_{\rm ext}(x,t) \to 0$ as $|x| \to \infty$]. In many experiments the condensate is put into motion with respect to the obstacle by resonant pumping. Here we rather describe a situation with nonresonant pumping, where condensation can be forced to occur in a finite-momentum state by seeding the system with a short coherent-light pulse.[26] However, we believe that the gross features of the theoretical study of the wave patterns and of the drag force are not essentially affected by the technique used for setting the fluid into motion. This is supported by a comparison of the results of the present work with the one of Ref. 29 where a continuous transition at a critical velocity (possibly different from the speed of sound) is also observed in a perturbative study of a resonantly driven polariton fluid.

As just discussed, in typical experiments with polariton condensates, the obstacle does not move and instead the condensate is put into motion with some velocity V. However we shall sometimes use for convenience a reference frame in which the condensate is at rest (far enough from the obstacle) and where the obstacle moves with velocity $-V$: $U_{\rm ext}(x,t) = f_{\rm ext}(x + Vt)$. A comprehensive study of this problem can be done in the case of an obstacle represented by a weak potential which induces a wave disturbance corresponding to small modifications of the parameters of the flow. In this configuration the problem can be treated in the framework of perturbation theory which is presented in Sec. III of the paper; this corresponds to the extension to damped systems of previous perturbative studies of BEC atomic vapors.[30–33] Note that the possibility of a perturbative treatment of Eq. (1) has already been foreseen in Refs. 26 and 34; this led to the identification of the relevant complex wave vectors involved in the perturbative analysis. In Sec. IV we consider the wave pattern generated by the flow of a polariton condensate past a *strong* obstacle potential, when perturbation theory no longer applies. In this case, it is appropriate to distinguish between *wide* and *narrow* obstacles depending on the ratio of their sizes to the healing length ξ (ξ is the de Broglie wavelength of polaritons moving with the sound velocity; see its definition in the next paragraph). When a narrow obstacle moves at supersonic speed the downstream profile has a rather smooth behavior which can be described by a dispersionless approach, the hydraulic approximation which we present in Sec. IV A. On the other hand, the upstream-wave structure can be represented (for small enough damping coefficient) as a weakly modulated nonlinear periodic wave which is a damped dispersive shock wave. Such shocks have been studied for the case of a wide obstacle with the use of Whitham modulation theory in Ref. 35. We present here a similar and more detailed study in the case of a δ impurity in Sec. IV B.

In the absence of external potential, a homogeneous and stationary solution of Eq. (1) corresponds to an order parameter of the form $\psi(x,t) = \sqrt{\rho_0}\exp(-i\mu t/\hbar)$, where ρ_0 is the uniform density and μ is the chemical potential. Inserting this expression in Eq. (1) one finds $\rho_0 = \gamma/\Gamma$ (necessary for obtaining a real μ corresponding to a time-independent density) and $\mu = \alpha\rho_0$. The characteristic density ρ_0 and energy μ are associated to characteristic velocity and distance, namely the speed of sound[36] $c_s = \sqrt{\alpha\rho_0/m}$ and the healing length $\xi = \hbar/(mc_s)$.

We will see below that, for a given obstacle potential $U_{\rm ext}(x,t)$, the flow pattern is monitored by only two dimensionless parameters: The Mach number M and the damping parameter η defined as

$$M = \frac{V}{c_s} \quad \text{and} \quad \eta = \frac{\gamma}{\mu}. \tag{2}$$

Having identified the relevant parameters of the problem one can simplify the notations by expressing densities in units of ρ_0, distances in units of ξ, times in units of ξ/c_s and energies in units of μ. In these new variables Eq. (1) takes the form

$$i\,\psi_t = -\tfrac{1}{2}\psi_{xx} + (U_{\rm ext}(x,t) + \rho)\psi + i\eta(1-\rho)\psi. \tag{3}$$

From now on, we shall use this dimensionless form of the damped Gross-Pitaevskii equation.

III. FLOW PAST A WEAK OBSTACLE

A. General linearized theory

In the absence of external potential Eq. (3) admits a uniform stationary solution of the form $\psi(x,t) = \exp(-i\,t)$. If the potential of the obstacle is weak, one can evaluate the density and the flow velocity profiles of the polariton condensate perturbatively. In this case one looks for a solution of Eq. (3) of the form

$$\psi(x,t) = [1 + \varphi(x,t)]\exp(-i\,t), \tag{4}$$

assuming that $|\varphi(x,t)| \ll 1$. Linearizing Eq. (3) with respect to $\varphi(x,t)$ and $U_{\rm ext}(x,t)$ and introducing the Fourier transforms

$$\begin{bmatrix} u(q,\omega) \\ v(q,\omega) \\ \hat{U}_{\rm ext}(q,\omega) \end{bmatrix} = \int_{\mathbb{R}^2} dx\, dt \begin{bmatrix} \varphi(x,t) \\ \varphi^*(x,t) \\ U_{\rm ext}(x,t) \end{bmatrix} e^{-i(qx-\omega t)}, \quad (5)$$

one finds that $u(q,\omega)$ and $v(q,\omega)$ satisfy the following linear system:

$$\mathcal{L}\begin{pmatrix} u(q,\omega) \\ v(q,\omega) \end{pmatrix} = -\hat{U}_{\rm ext}(q,\omega)\begin{pmatrix} 1 \\ 1 \end{pmatrix}, \quad (6)$$

where

$$\mathcal{L} = \begin{pmatrix} \frac{q^2}{2} - \omega + 1 - i\eta & 1 - i\eta \\ 1 + i\eta & \frac{q^2}{2} + \omega + 1 + i\eta \end{pmatrix}. \quad (7)$$

When $\hat{U}_{\rm ext}(q,\omega) \equiv 0$, that is, in the absence of the external obstacle, nontrivial solutions $u(q,\omega)$ and $v(q,\omega)$ of the 2×2 system (6) exist only when the determinant

$$D(q,\omega) = q^2\left(1 + \frac{q^2}{4}\right) - \omega^2 - 2i\eta\,\omega \quad (8)$$

of the matrix $\mathcal{L}$ is identically null. The resolution of the characteristic equation $D(q,\omega) = 0$ yields the dispersion relation $\omega(q)$ of the elementary excitations propagating on top of a homogeneous and stationary profile. Let us first consider the case $\eta \to 0$ (and also in dimensional units $\Gamma \to 0$ in such a way that the density $\rho_0 = \gamma/\Gamma$ is kept constant). In this case one finds that the excitation spectrum is the Bogoliubov one, that is, one recovers the dispersion relation of elementary excitations of a weakly interacting atomic Bose gas: $\omega(q) = \pm\omega_{\rm B}(q)$, where

$$\omega_{\rm B}(q) = q\sqrt{1 + \frac{q^2}{4}}. \quad (9)$$

In the case where η is not zero one gets[22]

$$\omega(q) = \begin{cases} -i\eta \pm i\sqrt{\eta^2 - \omega_{\rm B}^2(q)} & \text{if } |q| < q_*, \\ -i\eta \pm \sqrt{\omega_{\rm B}^2(q) - \eta^2} & \text{if } |q| > q_*, \end{cases} \quad (10)$$

where

$$q_* = \left[2(\sqrt{1+\eta^2} - 1)\right]^{1/2}. \quad (11)$$

In the ideal case ($\eta = 0$ and then $q_* = 0$) long-wavelength perturbations ($|q| \ll 1$) correspond to sound waves with a linear dispersion $\omega_{\rm B}(q) \simeq q$ and with a sound velocity equal to unity in our dimensionless units. As announced in note 36, perturbations with $|q| < q^*$ do not propagate in the presence of finite damping ($\eta \neq 0$). However, for small η there exists a finite region of wave number ($q_* \ll |q| \ll 1$) for which the dispersion relation (10) can be approximated by the long-wavelength limit $\omega(q) \simeq q - i\eta$ describing weakly damped sound waves.

Let us now consider the general case where $U_{\rm ext}(x,t)$ is not zero: The linear waves are generated by the external potential and their Fourier components $u(q,\omega)$ and $v(q,\omega)$ can be expressed by means of Eq. (6) in terms of this potential. This yields the following expression for the first-order density modulation $\delta\rho = \varphi + \varphi^*$ induced by $U_{\rm ext}(x,t)$:

$$\delta\rho(x,t) = \int_{\mathbb{R}^2} \frac{dq\, d\omega}{(2\pi)^2}\, \chi(q,\omega)\, \hat{U}_{\rm ext}(q,\omega)\, e^{i(qx-\omega t)}, \quad (12)$$

where

$$\chi(q,\omega) \equiv \frac{\delta\hat{\rho}(q,\omega)}{\hat{U}_{\rm ext}(q,\omega)} = -\frac{q^2}{D(q,\omega)} \quad (13)$$

is the linear response function of the system. A configuration of great experimental interest corresponds to the case where the condensate moves at constant velocity with respect to a static obstacle. In this case, in the frame where the condensate is at rest, the external potential is of the form

$$U_{\rm ext}(x,t) = f_{\rm ext}(x + Mt), \quad (14)$$

where M is, in our dimensionless units, the velocity of the obstacle with respect to the condensate. For being specific, we shall henceforth consider the case $M > 0$ which corresponds to an obstacle moving to the left in a frame where the condensate is at rest. Denoting by $\hat{f}_{\rm ext}$ the Fourier transform of $f_{\rm ext}$ [i.e., $\hat{f}_{\rm ext}(q) = \int_{\mathbb{R}} dz\, f_{\rm ext}(z) \exp(-iqz)$] the expression of $\delta\rho(x,t)$ in the case of an external potential of the form (14) reads

$$\begin{aligned} \delta\rho(x,t) &= \int_{\mathbb{R}} \frac{dq}{2\pi}\, \chi(q,-Mq)\, \hat{f}_{\rm ext}(q)\, e^{iq(x+Mt)} \\ &= \int_{\mathbb{R}} dz\, K(x+Mt-z)\, f_{\rm ext}(z), \end{aligned} \quad (15)$$

where

$$K(X) = \int_{\mathbb{R}} \frac{dq}{2\pi}\, \chi(q,-Mq)\, e^{iqX}. \quad (16)$$

One can first remark that $\delta\rho$ is a function of $x + Mt$ only: The perturbative approach predicts that the density modulations induced by an obstacle moving at constant velocity are stationary in the reference frame where the obstacle is at rest. Note however that, in the absence of damping, experiments performed on atomic condensates[7] and theory[31,32,37] show that there is a regime of time-dependent flows for impurity velocities close to the speed of sound. This is a nonlinear effect which is missed by the perturbative approach. In the presence of damping this time-dependent behavior also exits but, in a numerical study of nonlinear effects in the presence of a wide obstacle, it is observed in a smaller domain in the parameter space (Intensity of $U_{\rm ext}, V$) than when $\eta \equiv 0$.[35] This is confirmed in the case of a narrow obstacle by the numerical results of Sec. IV C below. In this respect, the perturbative result—being stationary—is thus more sound in the presence of damping since in this case the domain of time-dependent flows is reduced. We make this discussion quantitative at the end of Sec. III B by discussing the parameters governing the mathematical validity of perturbation theory.

A particular property of solution (15) comes from the conservation equation

$$\rho_t + j_x = 2\eta\,\rho\,(1-\rho), \quad (17)$$

where $j = {\rm Im}(\psi^*\psi_x)$ is the particle current-density. Actually, Eq. (17) is a *bona fide* conservation equation only when $\eta = 0$. For nonzero η, the number of particles is not conserved and Eq. (17) should rather be called a "nonconservation"

equation for the current of particles. Equation (17) is a direct consequence of (1); in the stationary regime it implies[23,35]

$$\int_{\mathbb{R}} dx\, \rho\,(1-\rho) = 0. \tag{18}$$

At the perturbative level this reads $\int_{\mathbb{R}} dx\, \delta\rho = 0$ which is trivially verified by (15).

B. Perturbative flow past a δ impurity

It is instructive to discuss in greater details the characteristics of the wave pattern induced by a localized obstacle represented by the potential

$$U_{\rm ext}(x,t) = \varkappa\,\delta(x+Mt). \tag{19}$$

Then one gets

$$\delta\rho(x,t) = \varkappa\, K(X = x+Mt), \tag{20}$$

where $K(X)$ is defined in Eq. (16). This density modulation is typical for the perturbations induced by a narrow obstacle moving in the polariton condensate. Besides, the solution of the δ-impurity problem is particularly interesting because $K(X)$ is the Green function from which the result for any potential is obtained by convolution [cf. Eq. (15)].

The integral (16) can be computed by the method of residues and $K(X)$ has different behaviors depending on the value of M and corresponding to different arrangements of the poles of $\chi(q,-Mq)$ in the complex q plane. The poles are the roots of the equation $D(q,-Mq)/q = 0$ which reads

$$q^3 + 4(1-M^2)q + 8i\eta M = 0. \tag{21}$$

The explicit expression of the three poles q_1, q_2, and q_3 as a function of η and M is given in Appendix A. One obtains the following generic expression (valid for all M):

$$K(X) = i\sum_{\ell=1}^{3} \mathrm{sgn}(\mathrm{Im}\, q_\ell)\,\mathrm{Res}(q_\ell)\,\Theta[\mathrm{sgn}(\mathrm{Im}\, q_\ell)X]\, e^{iq_\ell X}, \tag{22}$$

where Θ is the Heaviside step function and $\mathrm{Res}(q_\ell)$ is the residue of $\chi(q,-Mq)$ at q_ℓ ($\ell \in \{1,2,3\}$):

$$\mathrm{Res}(q_\ell) = \frac{-4\,q_\ell}{3q_\ell^2 + 4(1-M^2)}. \tag{23}$$

There exists a critical velocity $M_{\rm crit}$ below which the three poles of $\chi(q,-Mq)$ are all located on the imaginary axis (cf. Fig. 1 and also Appendix A) and in this case formula (22) shows that $K(X)$ exponentially goes to 0 when $|X| \to \infty$. A more transparent expression can be obtained by explicitly solving the third degree equation (21). For $M < M_{\rm crit}$ this yields

$$\begin{aligned} K(X \leqslant 0) &= -\frac{2}{A}\left[\frac{A-B}{A-3B}\, e^{(A-B)X} - \frac{4AB}{A^2-9B^2}\, e^{2BX}\right], \\ K(X \geqslant 0) &= -\frac{2}{A}\,\frac{A+B}{A+3B}\, e^{-(A+B)X}, \end{aligned} \tag{24}$$

where A and B are positive real numbers ($A > B \geqslant 0$) depending on M and η, whose expressions are given in Appendix A [Eq. (A3)].

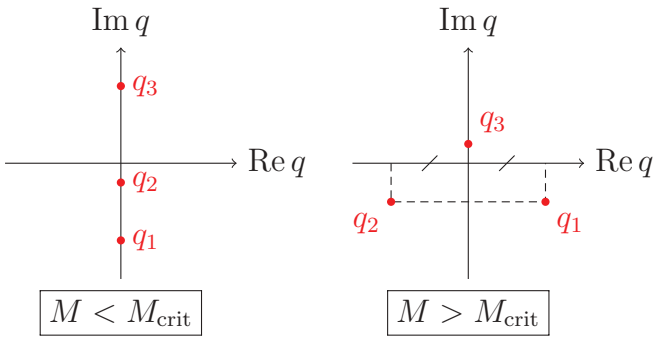

FIG. 1. (Color online) Location of the three poles q_1, q_2, and q_3 of $\chi(q,-Mq)$ in the complex q plane. For positive (negative) $X = x+Mt$ the integral in Eq. (16) is evaluated by closing the contour from above (below). As a result, for $M > M_{\rm crit}$ (damped) density oscillations are observed upstream from the obstacle (i.e., for $X < 0$).

On the other hand, when $M > M_{\rm crit}$, two of the poles acquire a real part and are symmetrically disposed with respect to the imaginary axis (cf. Fig. 1). In this case the wave pattern is given by the explicit formulas

$$\begin{aligned} K(X \leqslant 0) &= -\frac{4}{E}\,\mathrm{Im}\left(\frac{E-iF}{E-3iF}\, e^{iEX}\right) e^{FX}, \\ K(X \geqslant 0) &= -\frac{8F}{E^2+9F^2}\, e^{-2FX}, \end{aligned} \tag{25}$$

where the expression of the positive real numbers E and F is given in Eq. (A6).

The transition from one regime to the other takes place when two roots of Eq. (21) (namely q_1 and q_2) collide on the imaginary axis, that is, when the discriminant of this equation vanishes. This condition yields the expression of $M_{\rm crit}$:

$$M_{\rm crit}^2 = 1 - \frac{3}{2}\,\eta^{2/3}\left[(\sqrt{1+\eta^2}+1)^{1/3} - (\sqrt{1+\eta^2}-1)^{1/3}\right]. \tag{26}$$

When $\eta \to 0$, that is, in the absence of damping, one recovers the usual Landau threshold for emission of Cherenkov radiation in a weakly interacting Bose gas: $M_{\rm crit} = 1$ (in dimensional units, $V_{\rm crit} = c_s$). In this case, the perturbative treatment states that the flow is nondissipative for velocities below $M_{\rm crit}$ and dissipative above (see Refs. 32 and 33 and the computation of the drag in Sec. III D). This is identical to Landau's criterion since both approaches give the same value of velocity for the onset of dissipation and have the same physical content: Excitation of small nonlocalized perturbations is allowed only above $M_{\rm crit}$.

In the presence of dissipation $\eta \neq 0$, and Eq. (26) shows that $M_{\rm crit}$ is a decreasing function of η (cf. Fig. 2). For $M < M_{\rm crit}$ (subcritical velocities) there is no Cherenkov radiation but, as shown by the explicit computation of the drag force below, contrarily to the $\eta = 0$ case, the dissipative effects associated with the finite lifetime of polaritons induce a finite drag force on the obstacle and the flow is not strictly superfluid. For $M > M_{\rm crit}$, Cherenkov radiation becomes possible but dissipation within the condensate induces decay of the associated density oscillations. The corresponding density patterns are represented in each case ($M \lessgtr M_{\rm crit}$) in the insets of Fig. 2

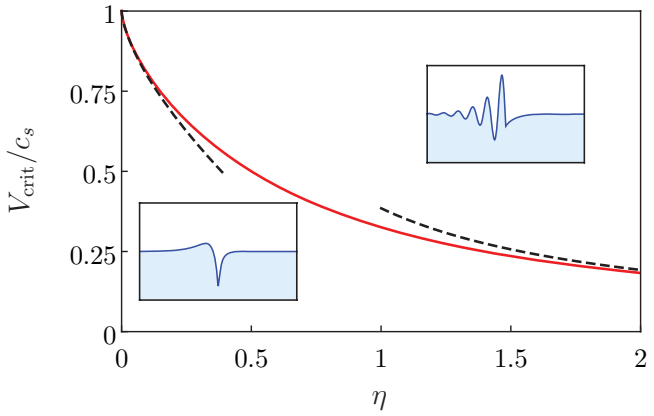

FIG. 2. (Color online) $M_{\rm crit} = V_{\rm crit}/c_s$ as a function of the dimensionless damping parameter η, such as given by Eq. (26). The dashed lines correspond to the asymptotic expressions $M_{\rm crit} \simeq 1 - \frac{3}{2}(\eta/2)^{2/3}$ (for low η) and $M_{\rm crit} \simeq 2/(3\sqrt{3}\,\eta)$ (for large η). The insets represent typical density profiles in the presence of a repulsive δ-peak impurity for $M < M_{\rm crit}$ (lower left inset) and $M > M_{\rm crit}$ (upper right inset).

and the relevant analytical expressions are given by Eqs. (24) and (25).

The fact that $M_{\rm crit}$ is modified by damping physically explains why perturbation theory is more accurate in the presence of damping. For a nondamped system, an obstacle moving at velocity close to $M_{\rm crit} = 1$ generates Bogoliubov excitations whose typical velocity is also close to $c_s = 1$. As a result, the perturbations accumulate in the vicinity of the obstacle (since they propagate at the same velocity), nonlinear effects cannot be neglected, and the perturbative approach fails.[38] In the presence of damping the critical velocity $M_{\rm crit}$ for radiating Cherenkov waves differs from the velocity of propagation of small amplitude perturbation and, moreover, the damping prevents large increases of the density. As a result there is no pile up of fluctuations in the vicinity of the obstacle, nonlinear effects may be neglected and the perturbative treatment is more likely to be valid.

This intuitive explanation of the increased accuracy of perturbation theory in the presence of damping is sustained by the mathematical reasoning we present now. In the absence of damping the amplitude of the relative density perturbation is of typical magnitude $\varkappa/|M^2-1|^{1/2}$ (i.e., perturbation theory indeed seriously fails when the velocity of the obstacle is close to the speed of sound[31] because the expression for $\delta\rho$ diverges). This problem is partially cured in the presence of damping: For a potential of the form (19) a possible estimate of the amplitude of $|\delta\rho(x,t)|$ is its value $\varkappa\,|K(0)|$ at the position of the obstacle. A study of the dependence of this quantity on the velocity and on the damping (i.e., on the dimensionless parameters M and η) shows that, for a fixed value of η, it typically reaches its largest value when $M = M_{\rm crit}$. The value of the quantity $\varkappa\,|K(0)|$ at $M = M_{\rm crit}$ is thus the small parameter ϵ of the perturbation expansion, in the sense that if this quantity is small for given $\varkappa$ and η, the perturbation theory is valid *for all velocities*. This condition reads [see formula (A10)] $\epsilon \equiv \varkappa/(1-M_{\rm crit}^2)^{1/2} \ll 1$. Hence ϵ is the small parameter of the perturbation theory in the presence of damping. It never diverges for finite η and this shows that perturbation theory is more sound with than without damping. We see that ϵ effectively decreases in the presence of damping because $M_{\rm crit}$ differs from 1, as advocated in the intuitive discussion of the previous paragraph. For small η, Eq. (A10) yields $\epsilon \propto \varkappa\,\eta^{-1/3}$ whereas for large η one finds $\epsilon \propto \varkappa$. One can thus equivalently define the small parameter of the theory as

$$\epsilon = \varkappa \times \max\{1, \eta^{-1/3}\}, \tag{27}$$

and indeed a numerical check shows that, at fixed η, ϵ as defined by (27) is a good estimate of the maximum value of $|\delta\rho(x)|$ for $x \in \mathbb{R}$ and $M \in \mathbb{R}_+$.

We stress that the condition $\epsilon \ll 1$ is a criterion of applicability of perturbation theory *for all* M at fixed η and $\varkappa$. It is a strong requirement: For given η and $\varkappa$ failing to fulfill the condition $\epsilon \ll 1$, there are still some velocities for which perturbation theory holds. For instance in the supersonic regime, when $\eta M(M^2-1)^{-3/2} \ll 1$, the condition of applicability of perturbation theory relies on the smallness of the upstream oscillations and reads $\varkappa/(M^2-1)^{1/2} \ll 1$ which is verified for large M even when ϵ is not small.

C. Generic flow pattern for a weak obstacle

For an obstacle of the generic form (14) the position of the poles of the response function and the critical velocity (26) play the same crucial role as for a δ impurity. Equation (15) yields the following explicit expression for the density oscillations:

$$\delta\rho(X) = i\int_{-\infty}^{X} dy\ \mathrm{Res}(q_3)\, f_{\rm ext}(y)\, e^{iq_3(X-y)} - i\int_{X}^{\infty} dy \sum_{\ell\in\{1,2\}} \mathrm{Res}(q_\ell)\, f_{\rm ext}(y)\, e^{iq_\ell(X-y)}, \tag{28}$$

where we recall that $\mathrm{Res}(q_\ell)$ is the residue of $\chi(q,-Mq)$ at q_ℓ ($\ell = 1, 2$ or 3) [see Eq. (23)]. Formula (28) is valid both below and above $M_{\rm crit}$. When $\eta = 0$ it reduces to the one already obtained in Ref. 31 in the absence of damping [Eq. (45) of this reference].

It is interesting to obtain from (28) the generic form of the long-distance wake which exists ahead of the obstacle when $M > M_{\rm crit}$. When X is negative and much larger than the range of the obstacle potential $f_{\rm ext}$, the first term in Eq. (28) can be neglected. If, furthermore, $f_{\rm ext}$ decreases rapidly enough at $-\infty$ so that $\hat{f}_{\rm ext}(q_{1,2})$ exists (typically when $f_{\rm ext}(x)$ decreases more rapidly than $\exp[-\mathrm{Im}(q_{1,2})\,x]$), one can approximate the second integral by a compact expression yielding

$$\delta\rho(X) \underset{X\to-\infty}{\simeq} 2\,\mathrm{Im}\big[\mathrm{Res}(q_1)\,\hat{f}_{\rm ext}(q_1)\,e^{iq_1X}\big]. \tag{29}$$

We recall that Eq. (29) is an approximation of formula (28) valid for $M > M_{\rm crit}$. It is of course exact for all $X \leqslant 0$ in the case of a δ impurity. It describes Cherenkov oscillations which are damped by a factor $\exp[-\mathrm{Im}(q_1)\,x]$, in complete agreement with the results obtained in Ref. 35 both numerically and also by means of Whitham averaging method [Eq. (42) of this reference].

Note that for large velocities ($M \gg M_{\rm crit}$) the imaginary parts of q_1 and q_2 tend to zero (cf. Appendix A) and the wake (29) thus extends far ahead from the obstacle: The effective damping of the Cherenkov radiation tends to zero. However,

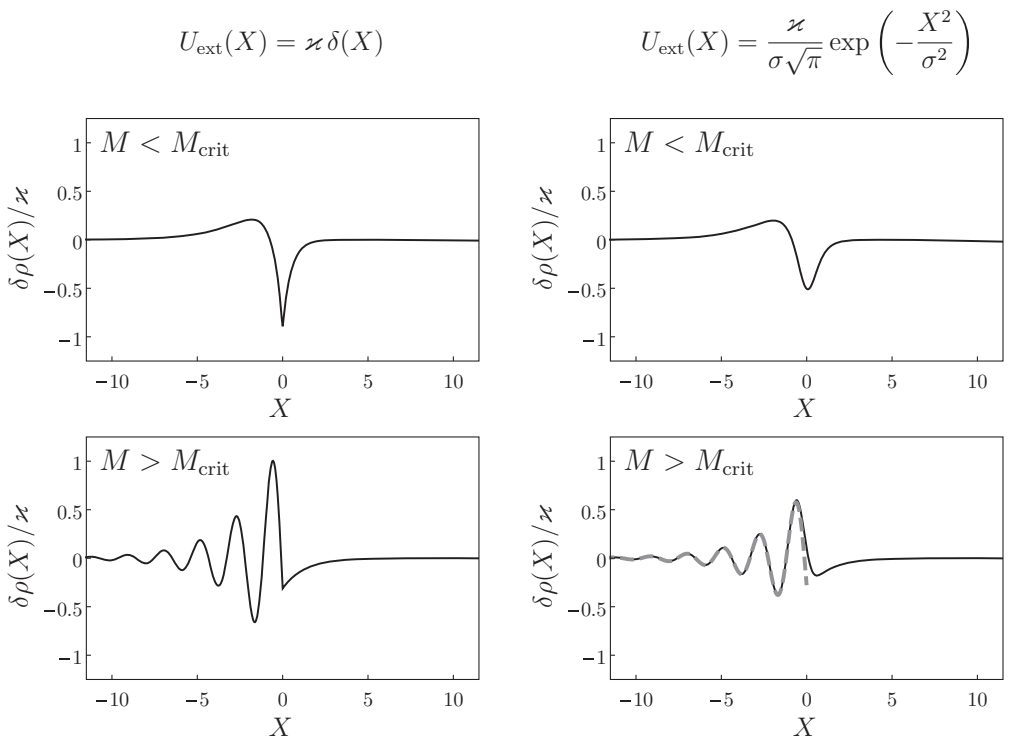

FIG. 3. $\delta\rho(X = x + Mt)$ for a δ-impurity potential (left panels) and a Gaussian potential (30) of width $\sigma = 0.5$ (right panels) as given by perturbation theory [Eq. (15)]. The plots are drawn for a system in which $\eta = 0.5$ and in this case $M_{\rm crit} = 0.5$. The two upper panels correspond to a velocity below $M_{\rm crit}$ ($M = 0.4$) and the two lower ones to a velocity above $M_{\rm crit}$ ($M = 1.75$). In the lower right panel the dashed gray line corresponds to the approximation (29).

in this limit, $|q_1|$ gets very large (cf. Appendix A) and for a generic potential $|\hat{f}_{\rm ext}(q_1)|$ becomes very small: The amplitude of the wake decreases uniformly at large velocity, not because of damping, but because the large kinetic energy of the flow with respect to the obstacle allows one to treat this obstacle as a small perturbation. The same effect had been predicted for BEC of ultracold vapors in Ref. 31 and has been observed experimentally in Refs. 7 and 8.

For being specific, we compare in Fig. 3 the density modulations obtained within perturbation theory for a δ-impurity obstacle (19) with the ones corresponding to a Gaussian potential of finite width σ:

$$U_{\rm ext}(x,t) = \frac{\varkappa}{\sigma\sqrt{\pi}} \exp\left[-\frac{(x+Mt)^2}{\sigma^2}\right]. \tag{30}$$

When $\sigma \to 0$ this potential tends to the δ-impurity potential (19). As just explained, when $M > M_{\rm crit}$ the damping of the oscillatory wake in front of the obstacle is more effective in the Gaussian case than for the δ impurity and is very well described by the asymptotic form (29) as shown in the lower right panel of Fig. 3.

D. Drag force

In order to discuss the precise influence of the finite lifetime of the polaritons on the possible superfluidity of the flow, it is interesting to compute the drag force F_d experienced by the obstacle. F_d is defined as[32]

$$F_d = \int_{\mathbb{R}} dx\, |\psi(x,t)|^2\, \partial_x U_{\rm ext}(x,t). \tag{31}$$

A natural way to compute F_d is to insert the perturbative expression (15) for $\delta\rho$ in Eq. (31) (see, e.g., Ref. 33). Another convenient way is to use the stress tensor $T(x,t)$ in a manner similar to what has been done in Ref. 32. The stress tensor is defined as

$$T(x,t) = -{\rm Im}(\psi^*\psi_t) + \tfrac{1}{2}|\psi_{xx}|^2 - \tfrac{1}{2}\rho^2 - \rho\, U_{\rm ext}. \tag{32}$$

It verifies the "nonconservation" equation

$$J_t + T_x + \rho(U_{\rm ext})_x = 2\eta\,(1-\rho)\,J, \tag{33}$$

where in dimensionless units the momentum current-density J coincides with the particle current-density: $J(x,t) \equiv j(x,t)$. In the presence of damping, in the stationary regime, integrating this expression over position, one gets

$$F_d = 2\eta \int_{\mathbb{R}} dx\,(1-\rho)\,J. \tag{34}$$

Within the perturbative approach one can show that $J(X = x + Mt) = -M\,\delta\rho(X) - 2\eta\int_{-\infty}^{X} dy\,\delta\rho(y)$, and using the result (18) this yields, for an obstacle of type (14),

$$\begin{aligned} F_d &= 2\eta\, M \int_{\mathbb{R}} dx\,[\delta\rho(x)]^2 \\ &= 2\eta\, M \int_{\mathbb{R}} \frac{dq}{2\pi}\, |\chi(q,-Mq)|^2\, |\hat{f}_{\rm ext}(q)|^2. \end{aligned} \tag{35}$$

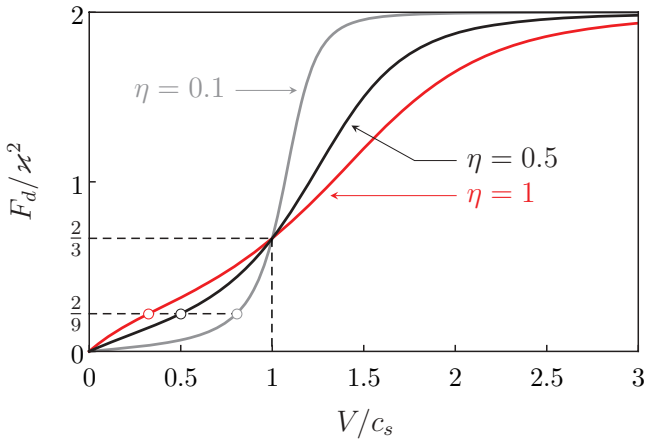

FIG. 4. (Color online) $F_d/\varkappa^2$ as a function of $M = V/c_s$ for different values of the dimensionless damping parameter η. The curves are drawn for the δ-impurity potential (19): $U_{\rm ext}(X) = \varkappa\,\delta(X)$. For each curve the abscissa of the white dot spots the value of $M_{\rm crit}(\eta)$. For each η this critical velocity is reached exactly when $F_d/\varkappa^2 = \frac{2}{9}$.

We emphasize that (31) is generally valid, that (34) is only valid for a stationary regime in the presence of damping for an obstacle moving at constant velocity, and that (35) is the perturbative evaluation of (34).

For concreteness we now give the explicit expression of the perturbative drag (35) in the case where the potential is a Dirac peak of the form (19). One gets

$$F_d = -\frac{\varkappa^2}{2} \sum_{\ell\in\{1,2,3\}} \mathrm{sgn}(\mathrm{Im}\, q_\ell)\, q_\ell\, \mathrm{Res}(q_\ell). \tag{36}$$

Substitution of the explicit expressions for the poles yields

$$F_d = \frac{\varkappa^2 \eta\, M (1-M^2)^{-3/2}}{\cos\frac{\theta}{3}\left(\cos\frac{\theta}{3} + \frac{1}{\sqrt{3}}\sin\frac{\theta}{3}\right)\left(\cos\frac{\theta}{3} + \sqrt{3}\sin\frac{\theta}{3}\right)}, \tag{37}$$

for $M < M_{\rm crit}$ and

$$F_d = \frac{8\,\varkappa^2 \eta\, M}{F(E^2 + 9F^2)} \tag{38}$$

for $M > M_{\rm crit}$ [in the above expressions θ, E, and F are given by Eqs. (A1) and (A6)]. The behavior of F_d as a function of M is displayed in Fig. 4 for several values of η. For each η the critical velocity $M_{\rm crit}$ is reached exactly when the drag is $F_d = 2\varkappa^2/9$. The corresponding points are shown as white dots in the figure. One can also show that for all η one has $F_d = 2\varkappa^2/3$ when $M = 1$.

From formulas (36), (37), and (38) one finds

$$F_d \simeq \varkappa^2 \times \begin{cases} \eta M & \text{when} \quad M \to 0, \\ 2 & \text{when} \quad M \to \infty, \end{cases} \tag{39}$$

in agreement with the main features of Fig. 4. It is interesting to notice that the drag force is proportional to ηM when $M \to 0$ (a similar behavior has already been observed in Refs. 26 and 29). This means that at low velocity the obstacle experiences a force which is similar to a viscous drag of Stokes type: (i) it is proportional to the velocity; (ii) it is linked to diffusion of momentum as shown in the polariton case by Eq. (33) and by the fact that the associated wave vector is imaginary.

When M increases and reaches the value $M = M_{\rm crit}$, a wake begins to be emitted ahead of the obstacle. It consists of (damped) Cherenkov radiations and one could say, pursuing the analogy with fluid mechanics, that this marks the onset of wave resistance. One can push the analogy one step further and compare the present results with the ones obtained in experimental studies of the drag force exerted on objects moving at the surface of several viscous fluids. In such experiments it is typically observed, as in Fig. 4, that the transition to the wave drag is continuous,[39] but also that F_d considered as a function of V has a quasidiscontinuous behavior for decreasing viscosity.[40] An exactly discontinuous behavior is typical for the perturbative drag in superfluids[32] and is also expected on the basis of Raphaël-de Gennes theory of wave resistance in the context of capillary-gravity waves at the surface of inviscid fluids.[41] This discontinuity disappears for finite viscosity.[42] Moreover, it is interesting to remark that from Fig. 4 one might erroneously guess (as is sometimes done in the analysis of fluid mechanics experiments) that the relevant critical velocity for the onset of wave drag does not depend on viscosity (i.e., on η in our case) and that at finite viscosity the behavior of $F_d(M)$ is just smoothed around the inviscid value [$2\varkappa^2\Theta(M-1)$ in our case]. From our analytical analysis we know that in reality the wave drag sets in at $M_{\rm crit}$ [which is not equal to the inviscid value $M_{\rm crit}(\eta = 0) = 1$] and that it is not possible, when $M \simeq M_{\rm crit}$ or 1, to disentangle in the expression of F_d a viscous component from a wave resistance. This is clear from Fig. 4 where the onset of wave drag is shown by thick white dots: At these points F_d remains a smooth function of M.

In Fig. 4 all curves merge at $M = 1$, and it is intriguing to remark that the drag for a fixed velocity M larger than unity decreases for increased damping. This counterintuitive effect has already been observed in a study of the motion of nitrogen drops floating at the surface of a liquid bath.[42] It is explained by the fact that viscous effects reduce the range of the wake and accordingly diminish the wave resistance which is the dominant source of drag when $M > 1$.[43]

At large velocity all curves in Fig. 4 tend to the same constant value, which is the result for the drag force in the absence of damping. The fact that the large velocity drag does not depend on M is an artifact of the δ-impurity potential, as demonstrated by the results obtained in the more standard case where the obstacle is described by a Gaussian potential of the form (30). In this case formula (31) or (35) leads to the expression

$$F_d = -\frac{\varkappa^2}{2} \sum_{\ell\in\{1,2,3\}} q_\ell\, \mathrm{Res}(q_\ell)\, e^{-\sigma^2 q_\ell^2/2} \times \left[\mathrm{sgn}(\mathrm{Im}\, q_\ell) + \mathrm{erf}\left(\frac{i\sigma q_\ell}{\sqrt{2}}\right)\right]. \tag{40}$$

The corresponding curves are shown in Fig. 5. The counterintuitive η dependence already observed in the case of a δ-impurity potential is here even more striking: The maximum drag is larger at small η (compare the curves obtained for $\eta = 0.2$ and $\eta = 0.6$).

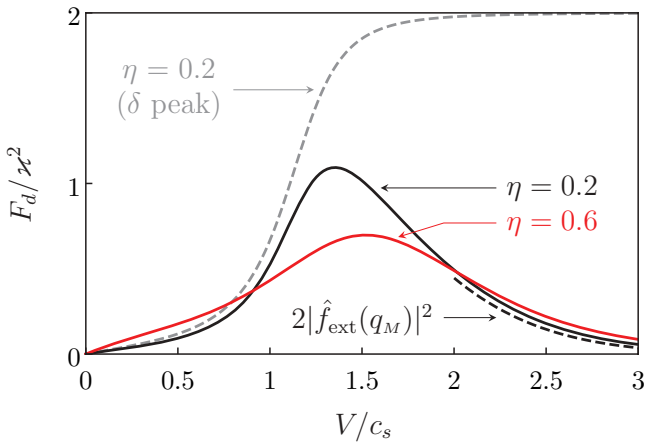

FIG. 5. (Color online) $F_d/\varkappa^2$ as a function of $M = V/c_s$ for different values of the dimensionless damping parameter η. The solid curves are drawn for a Gaussian-impurity potential of width $\sigma = 0.5$. The black dashed line is the corresponding asymptotic result (45). The gray dashed line is the result for a δ-impurity potential, shown for comparison.

In order to better understand the large-velocity behavior of the perturbative estimate of the drag force we now derive an explicit asymptotic expansion valid for any potential of the form (14) moving at large velocity. From expressions (15) and (31) one gets

$$F_d = -i\int_{\mathbb{R}} \frac{dq}{2\pi}\, q\, \chi(q,-Mq)\,|\hat{f}_{\rm ext}(q)|^2 = -i\int_{\mathbb{R}^2} dx\,\frac{dq}{2\pi}\, q\,\chi(q,-Mq)\, f_{\rm ext}\circ f_{\rm ext}(x)\, e^{-iqx}. \quad (41)$$

In Eq. (41) $f_{\rm ext}\circ f_{\rm ext}$ is the convolution of $f_{\rm ext}$ with itself. The integral over q in this formula can be evaluated by the method of residues. For positive (negative) x the contour has to be closed from below (above). Considering that when $M > M_{\rm crit}$ the poles q_1 and q_2 which lie in the lower half of the complex q plane verify $q_2 = -q_1^*$ and $\mathrm{Res}(q_2) = -[\mathrm{Res}(q_1)]^*$, one gets

$$F_d = -2\,\mathrm{Re}\left[q_1\,\mathrm{Res}(q_1)\int_0^\infty dx\, f_{\rm ext}\circ f_{\rm ext}(x)\, e^{-iq_1x}\right] + q_3\,\mathrm{Res}(q_3)\int_{-\infty}^0 dx\, f_{\rm ext}\circ f_{\rm ext}(x)\, e^{-iq_3x}. \quad (42)$$

At large velocity one obtains, from Eqs. (23) and (A8),

$$q_1\,\mathrm{Res}(q_1) = -2 + O\left(\frac{\eta M}{(M^2-1)^{3/2}}\right), \qquad q_3\,\mathrm{Res}(q_3) = O\left(\frac{\eta M}{(M^2-1)^{3/2}}\right). \quad (43)$$

From this, and using the fact that $f_{\rm ext}\circ f_{\rm ext}$ is an even function of x, one can cast the leading-order contribution to F_d in Eq. (42) under the form

$$F_d = 2\int_{\mathbb{R}} dx\, e^{-i\mathrm{Re}(q_1)x}\, e^{\mathrm{Im}(q_1)|x|}\, f_{\rm ext}\circ f_{\rm ext}(x) = 2\int_{\mathbb{R}}\frac{dq}{2\pi}\,\frac{-2\,\mathrm{Im}\,q_1}{[\mathrm{Re}(q_1)-q]^2+\mathrm{Im}^2 q_1}\,|\hat{f}_{\rm ext}(q)|^2. \quad (44)$$

The last expression in Eq. (44) is obtained using Parseval-Plancherel theorem. At large velocity the imaginary part of q_1 is of order $\eta M(M^2-1)^{-1}$, whereas its real part is $\mathrm{Re}\,q_1 \simeq q_M \equiv 2(M^2-1)^{1/2}$ [cf. Eq. (A8)]: The Lorentzian in Eq. (44) is thus a good approximation of the Dirac distribution $\delta(q-q_M)$. This directly yields the following large velocity result:

$$F_d = 2\,|\hat{f}_{\rm ext}(q_M)|^2\left[1 + O\left(\frac{\eta M}{(M^2-1)^{3/2}}\right)\right]. \quad (45)$$

This means that the typical drag depends on velocity (through q_M) and tends to zero at large velocity[44] contrarily to what occurs for the δ-impurity obstacle. It is interesting to notice that the result (45) does not depend on η at leading order (i.e., that the large-velocity drag corresponds to pure wave resistance). Besides, as already remarked in Sec. III C [paragraph between Eqs. (29) and (30)], the obstacle can always be treated as a perturbation at large velocity and the associated drag force decreases (the large velocity limit was accordingly denoted as "quasiideal" in Ref. 45).

We end this section by noting that the drag force has not only a methodological interest, but that it is also a measurable quantity. This is clear in the context of classical hydrodynamics.[39,40] This is also partially true in the context of Bose condensation where one can have an indirect grasp on F_d by measuring the rate of the part of energy dissipation associated with the force experienced by the obstacle[33,46]: $dE/dt = -MF_d$. For instance, the experiment of Raman *et al.*[4] demonstrates breaking of Landau criterion, not through the emission of a wake (which is present, but not measured), but by an increase of the measured thermal noncondensed fraction. This increase is due to the dissipation of the work done by the finite drag force.

IV. NONLINEAR THEORY FOR A NARROW OBSTACLE

In this section we present results valid for strong obstacle potentials, in regimes where the perturbative approach of the previous section typically fails. In the limit of small damping ($\eta \ll 1$) one can expect that other approximations are valid. For example, in the case of an obstacle represented by a strong δ potential, one can assume that the condensate is strongly disturbed at the location of the obstacle, so that the difference $1-\rho(0)$ is not small; however, the derivative of the distribution $\rho(x)$ downstream from the obstacle (for $x > 0$) is controlled by η and can be considered as small in the case of small damping. Hence we can develop for this region a so-called *hydraulic approximation* by neglecting higher order dispersive effects in our equations (see, e.g., Ref. 35). On the other hand, upstream from the obstacle (in the region $x < 0$) a supercritical flow generates a stationary oscillatory structure whose oscillation's amplitudes are not small, contrarily to what was assumed in the previous section. However, in the case of small η this oscillatory structure can be represented as a slowly modulated nonlinear wave and, hence, the *Whitham modulation theory* can be applied to its description. In this section we shall use these two approximate methods (hydraulic approximation and Whitham averaging technique) and compare their results with the exact numerical solution of the problem.

In all this section we restrict ourselves to the *stationary version* of Eq. (3) in the presence of a δ impurity. We find it more convenient to work in a reference frame where the obstacle is at rest while the condensate moves from left to right with an asymptotic velocity and density, respectively, equal to M and 1 at both infinities. The equation to be solved is the following:

$$\left(\frac{M^2}{2}+1\right)\psi = -\frac{1}{2}\psi_{xx} + (\varkappa\,\delta(x)+\rho)\psi + i\eta(1-\rho)\psi. \tag{46}$$

Contrarily to the case of a weak obstacle, where one can show that a stationary solution always exists within perturbation theory (see Sec. III A), it is not *a priori* evident that Eq. (46) admits a solution. Hence, the assumption of existence of a stationary nonlinear regime has to be validated by exhibiting the corresponding solution and demonstration of its stability. If such a solution cannot be found, this means that only time-dependent flows exist for the chosen values of η, $\varkappa$, and M, which are the three parameters characterizing the flow.

By means of the substitution

$$\psi(x) = \sqrt{\rho(x)}\exp\left[i\int^x dx'\,u(x')\right], \tag{47}$$

the Gross-Pitaevskii equation (46) can be cast—outside the range of action of the obstacle potential—into a hydrodynamic form for the rescaled density $\rho(x)$ and flow velocity $u(x)$:

$$\begin{aligned}(\rho\,u)_x &= 2\eta\,\rho\,(1-\rho),\\ \frac{u^2}{2}+\rho+\frac{\rho_x^2}{8\rho^2}-\frac{\rho_{xx}}{4\rho} &= \frac{M^2}{2}+1.\end{aligned} \tag{48}$$

We shall use these hydrodynamic notations in this section.

A. Hydraulic approximation in the downstream region of a supersonic flow

In the hydraulic approximation the derivatives are supposed to be small; hence we can neglect the two last terms in the left-hand side of the second of Eqs. (48) to get $u^2/2+\rho = M^2/2+1$. Then $u(x)$ can be expressed in terms of $\rho(x)$ and substituted into the first of Eqs. (48) to give

$$\left[\rho\sqrt{M^2+2(1-\rho)}\right]_x = 2\eta\,\rho\,(1-\rho). \tag{49}$$

The solution of this equation, with the boundary condition

$$\rho(0)\equiv\bar\rho, \tag{50}$$

can be easily expressed in terms of elementary functions:

$$\begin{aligned}x = \frac{1}{2\eta}\Bigg\{&\left(M-\frac{1}{M}\right)\ln\frac{(1-\bar\rho)\left[M^2+1-\rho+M\sqrt{M^2+2(1-\rho)}\right]}{(1-\rho)\left[M^2+1-\bar\rho+M\sqrt{M^2+2(1-\bar\rho)}\right]}\\ &-\sqrt{M^2+2}\ln\frac{\bar\rho\left[M^2+2-\rho+\sqrt{(M^2+2)(M^2+2(1-\rho))}\right]}{\rho\left[M^2+2-\bar\rho+\sqrt{(M^2+2)(M^2+2(1-\bar\rho))}\right]}\Bigg\}.\end{aligned} \tag{51}$$

This formula implicitly defines the dependence of the density ρ on x.

In the supersonic case, in the far downstream region, one has $1-\rho(x)\ll 1$ and one can linearize Eq. (49) with respect to $\delta\rho=\rho-1$. This yields[35]

$$|\delta\rho(x)| \propto \exp\left(-\frac{2\eta M}{M^2-1}\,x\right). \tag{52}$$

The perturbation theory used in the previous section predicts the same behavior when $\eta M(M^2-1)^{-3/2}\ll 1$ [$\delta\rho$ is found to be proportional to $\exp(iq_3x)$, where q_3 is given by (A8)]. However, the range of validity of Eq. (52) is different: The condition of smallness of the derivative yields the following condition of applicability of the hydraulic approximation:

$$\frac{\eta M}{M^2-1}\ll 1. \tag{53}$$

As a consequence of these different regimes of validity one can make the following remark: If $1-\bar\rho\ll 1$, the linearization of Eq. (49) can be extended down to $x=0$, yielding $\rho(x\geqslant 0)\simeq 1-(1-\bar\rho)\exp[-2\eta Mx/(M^2-1)]$. As we shall see in the numerical Sec. IV C, this approximation has a larger range of validity than the pure perturbation approach of Sec. III. This larger range of validity of the linearized version of (51) is a result of a drawback of the hydraulic approximation: The value of $\bar\rho=\rho(0)$ is not predicted by this method and has to be specified before comparison with numerical results. However, we will see in Sec. IV C that once this is done, Eq. (51) gives an excellent account of the downstream wave pattern with slow gradients in a supersonic flow.[47]

B. Whitham approximation in the upstream region of a supersonic flow

Upstream from the obstacle (when $x<0$) supercritical flows typically generate a dispersive shock wave which is the nonlinear version of the oscillatory wake observed in Sec. III. Now the amplitude of this wave cannot be considered as small, but for small η its parameters are poorly modified over one wavelength. Therefore we can describe such a flow within Whitham modulation theory which is a nonlinear adiabatic approach.[48]

In the absence of damping ($\eta=0$) the nonlinear progressive periodic wave solutions of (48) can be written in the form (see, e.g., Refs. 37 and 49):

$$\begin{aligned}\rho(x,t) = {}&\tfrac{1}{4}(\lambda_1-\lambda_2-\lambda_3+\lambda_4)^2+(\lambda_1-\lambda_2)(\lambda_3-\lambda_4)\\ &\times \mathrm{sn}^2\left(\sqrt{(\lambda_1-\lambda_3)(\lambda_2-\lambda_4)}\,(x-V_\varphi\,t),m\right),\end{aligned} \tag{54}$$

and

$$u(x,t) = V_\varphi + \frac{j}{\rho(x,t)}, \tag{55}$$

where sn is the sine elliptic Jacobi function,

$$V_\varphi = \frac{1}{2}\sum_{i=1}^{4}\lambda_i, \quad m = \frac{(\lambda_1-\lambda_2)(\lambda_3-\lambda_4)}{(\lambda_1-\lambda_3)(\lambda_2-\lambda_4)}, \tag{56}$$

and

$$\begin{aligned} j = {} & \tfrac{1}{8}(-\lambda_1-\lambda_2+\lambda_3+\lambda_4) \\ & \times(-\lambda_1+\lambda_2-\lambda_3+\lambda_4)(\lambda_1-\lambda_2-\lambda_3+\lambda_4). \end{aligned} \tag{57}$$

The parameters $\lambda_1 \leqslant \lambda_2 \leqslant \lambda_3 \leqslant \lambda_4$ are called the Riemann invariants of the system. In the case of strictly periodic solutions they are constant and they determine characteristics of the wave such as the phase velocity V_φ [Eqs. (56)], the current j evaluated in the frame where the wave is standing [Eq. (57)], the amplitude of the oscillations,

$$a = (\lambda_1-\lambda_2)(\lambda_3-\lambda_4), \tag{58}$$

and their wavelength,

$$L = \frac{2\,\mathrm{K}(m)}{\sqrt{(\lambda_1-\lambda_3)(\lambda_2-\lambda_4)}}, \tag{59}$$

$\mathrm{K}(m)$ being the complete elliptic integral of the first kind.

In the modulated dispersive shock wave occurring in the upstream region, the λ's become functions of position and time which vary weakly over one wavelength and one period. We consider here the stationary solution and in this case these parameters do not depend on time t and the phase velocity V_φ is equal to zero:

$$V_\varphi = \frac{1}{2}\sum_{i=1}^{4}\lambda_i = 0. \tag{60}$$

However, because η is not strictly zero, in the upstream region, even if the λ's do not depend on time they are functions of position and their x dependence is determined by the perturbed Whitham equations (see Appendix B):

$$\frac{d\lambda_i}{dx} = \frac{2}{L}\frac{G_1\lambda_i + G_2}{\prod_{m\neq i}(\lambda_i-\lambda_m)}, \quad i \in \{1,2,3,4\}, \tag{61}$$

where

$$\begin{aligned} G_1 &= -\eta\int_{\nu_1}^{\nu_2} d\nu\,\frac{\nu(1-\nu)}{\sqrt{\mathcal{R}(\nu)}}, \\ G_2 &= -\frac{\eta\sqrt{\nu_1\nu_2\nu_3}}{2}\int_{\nu_1}^{\nu_2} d\nu\,\frac{1-\nu}{\sqrt{\mathcal{R}(\nu)}}, \end{aligned} \tag{62}$$

$\mathcal{R}(\nu)$ and ν_1, ν_2, ν_3 being defined by Eqs. (B14) and (B15). According to Eq. (60), the system (61) admits the first integral $\sum_{i=1}^{4}\lambda_i = 0$. We shall now show that it admits another integral and can thus be reduced to a set of two (coupled) differential equations. To this end, we shall use the Jacobi identities

$$\begin{aligned} &\sum_{i=1}^{4}\frac{\lambda_i^k}{\prod_{m\neq i}(\lambda_i-\lambda_m)} = 0 \quad \text{for} \quad 0 \leqslant k \leqslant 2, \quad \text{and} \\ &\sum_{i=1}^{4}\frac{\lambda_i^3}{\prod_{m\neq i}(\lambda_i-\lambda_m)} = 1, \end{aligned} \tag{63}$$

to obtain $\frac{ds_1}{dx} = 0 = \frac{ds_2}{dx}$ and

$$\frac{ds_3}{dx} = \frac{2G_1}{L}, \quad \frac{ds_4}{dx} = -\frac{2G_2}{L}, \tag{64}$$

where the s's are symmetric functions of the λ's:

$$\begin{aligned} s_1 &= \sum_i \lambda_i, & s_2 &= \sum_{i<j}\lambda_i\lambda_j, \\ s_3 &= \sum_{i<j<k}\lambda_i\lambda_j\lambda_k, & s_4 &= \lambda_1\lambda_2\lambda_3\lambda_4. \end{aligned} \tag{65}$$

Here s_1 and s_2 are the integrals of our system. The value of s_1 is already known from Eq. (60): $s_1 = 0$. In order to determine the value of s_2 we calculate the asymptotic values of the Riemann invariants at $x \to -\infty$, where the flow is stationary with $\rho = \rho_0 = 1$ and $u = u_0 = M > 0$. The amplitude of the oscillations vanishes here; hence we find from (58) that $\lambda_1 = \lambda_2$ (another possible choice is $\lambda_3 = \lambda_4$; it corresponds to a flow with $M < 0$). Then, from Eq. (B15) we have the equation

$$\lim_{x\to-\infty}\rho(x) = \rho_0 = 1 = \nu_1 = \nu_2 = \tfrac{1}{4}(\lambda_3-\lambda_4)^2, \tag{66}$$

as well as the expression for the current density,

$$\lim_{x\to-\infty} j(x) = \rho_0 u_0 = M = \tfrac{1}{8}(\lambda_3-\lambda_4)^2(-2\lambda_1+\lambda_3+\lambda_4), \tag{67}$$

from which we get another equation:

$$M = \tfrac{1}{2}(-2\lambda_1+\lambda_3+\lambda_4). \tag{68}$$

With account of Eq. (60) (that is, $2\lambda_1+\lambda_3+\lambda_4 = 0$) we find, at $x \to -\infty$,

$$\lambda_1 = \lambda_2 = -\frac{M}{2}, \quad \lambda_3 = \frac{M}{2}-1, \quad \lambda_4 = \frac{M}{2}+1. \tag{69}$$

Hence,

$$s_2 = \mathrm{C}^{\mathrm{st}} = -\frac{M^2}{2} - 1. \tag{70}$$

From the definition (65) of the s_i's it is clear that the λ_i's are the solutions of the fourth degree equation $\lambda^4 - s_1\lambda^3 + s_2\lambda^2 - s_3\lambda + s_4 = 0$. The two parameters s_1 and s_2 having just been determined [$s_1 = 0$ and the value of s_2 is given in Eq. (70)] we can define the functions $\lambda_i = \lambda_i(s_3,s_4)$ as being the roots of the equation

$$\lambda^4 - \left(\frac{M^2}{2}+1\right)\lambda^2 - s_3\,\lambda + s_4 = 0, \tag{71}$$

ordered according to $\lambda_1 \leqslant \lambda_2 \leqslant \lambda_3 \leqslant \lambda_4$. Substitution of these functions into (B15) and of the results into (64) yields the system of two differential equations for s_3 and s_4,

$$\frac{ds_3}{dx} = \frac{2G_1(s_3,s_4)}{L(s_3,s_4)}, \quad \frac{ds_4}{dx} = -\frac{2G_2(s_3,s_4)}{L(s_3,s_4)}. \tag{72}$$

We now have to find the initial conditions for this system, that is, to determine the values of s_3 and s_4 at $x = 0$. To this end, we take into account that Whitham theory implies that the parameters of the wave weakly change over a distance of about one wavelength. Therefore we can assume that, to the left of the obstacle and close enough to it, the wave can be approximated

by the cnoidal wave solution (54), (55) and to the right of the obstacle it is given by a hydraulic approximation parametrized by the value $\bar{\rho}$ of the density at the location of the δ obstacle.

It is known (see, e.g., Ref. 49) that a nonmodulated cnoidal wave solution $\rho(x)$ satisfies the equation

$$\rho_x = 2\sqrt{\mathcal{R}(\rho)}, \tag{73}$$

where the coefficients of the polynomial

$$\begin{aligned}\mathcal{R}(v) &= (v-v_1)(v-v_2)(v-v_3)\\ &= v^3 + 2s_2v^2 + \left(s_2^2 - 4s_4\right)v - s_3^2\end{aligned} \tag{74}$$

are expressed in terms of the symmetric functions s_2, s_3, and s_4. Then the solution (54), (55) (with $V_\varphi = 0$) can be expressed in terms of the zeros v_1, v_2, v_3 of this polynomial as follows:

$$\begin{aligned}\rho(x) &= v_1 + (v_2 - v_1)\,\mathrm{sn}^2\left(\sqrt{v_3 - v_1}\,x, m\right),\\ u(x) &= \frac{s_3}{\rho(x)},\end{aligned} \tag{75}$$

where

$$m = \frac{v_2 - v_1}{v_3 - v_1} \quad \text{and} \quad L = \frac{2\,\mathrm{K}(m)}{\sqrt{v_3 - v_1}}. \tag{76}$$

In the stationary modulated situation we consider that v_1, v_2, v_3, s_3, m, and L do not depend on time in Eqs. (75) and (76), but they all depend on x.

It follows from Eq. (17) that the current of polaritons is preserved in transition through the δ potential: $j(0^-) = j(0^+)$. Then the second of Eqs. (75) yields (under the assumption that the hydraulic approximation is valid for $x \geqslant 0$ because $\eta \ll 1$) the value of $s_3(0)$:

$$s_3(0) = u(0)\rho(0) = \bar{\rho}\sqrt{M^2 + 2(1-\bar{\rho})}. \tag{77}$$

For calculating the value of $s_4(0)$ we use the matching condition at $x = 0$:

$$\rho_x(0^+) - \rho_x(0^-) = 4\varkappa\rho(0). \tag{78}$$

Pursuing the use of the downstream hydraulic approximation already used in Eq. (77) we write $\rho(0) = \bar{\rho}$ and, from Eq. (49),

$$\rho_x(0^+) = \frac{2\eta\,\bar{\rho}\,(1-\bar{\rho})\sqrt{M^2 + 2(1-\bar{\rho})}}{M^2 + 2 - 3\bar{\rho}}. \tag{79}$$

In the same spirit of a small-η approximation we have from Eq. (73) $\rho_x(0^-) = -2\sqrt{\mathcal{R}(\bar{\rho})}$, so that Eq. (78) reads

$$\mathcal{R}(\bar{\rho}) = \left[2\varkappa\bar{\rho} - \frac{\eta\,\bar{\rho}\,(1-\bar{\rho})\sqrt{M^2 + 2(1-\bar{\rho})}}{M^2 + 2 - 3\bar{\rho}}\right]^2. \tag{80}$$

This yields

$$\begin{aligned}&(v_1v_2 + v_2v_3 + v_3v_1)_{x=0}\\ &\quad = s_2^2 - 4s_4(0) = \frac{[4\varkappa\bar{\rho} - \rho_x(0^+)]^2}{4\bar{\rho}} + (2M^2 + 4 - 3\bar{\rho})\bar{\rho},\end{aligned} \tag{81}$$

and then

$$\begin{aligned}s_4(0) = \frac{1}{4}&\left[\frac{(M^2+2)^2}{4} - 2(M^2+2)\bar{\rho} + 3\bar{\rho}^2\right]\\ &-\bar{\rho}\left[\varkappa - \frac{\eta\,(1-\bar{\rho})\sqrt{M^2 + 2(1-\bar{\rho})}}{2(M^2 + 2 - 3\bar{\rho})}\right]^2.\end{aligned} \tag{82}$$

TABLE I. Values of $\bar{\rho}$ for different values of $\varkappa$ in the case $M = 3$ and $\eta = 0.05$. The row $\bar{\rho}$ (Whitham) corresponds to the value of $\bar{\rho} = \rho(0)$ found by solving Whitham Eqs. (83) and imposing the condition (85) (see the text). The row $\bar{\rho}$ (numerics) corresponds to the value of $\rho(0)$ found *via* a numerical resolution of Eq. (46).

$\varkappa$	0.5	1.0	1.5	2.0	2.5
$\bar{\rho}$ (Whitham)	0.9370	0.7932	0.6384	0.5056	0.4011
$\bar{\rho}$ (numerics)	0.9352	0.7916	0.6377	0.5055	0.4013

We note here that for small values of η, the analytical expression (82) can be simplified by replacing Eq. (79) by the simple approximation $\rho_x(0^+) = 0$. This amounts to also replacing η by 0 in the expressions (80) and (82). This simple scheme is accurate when $\eta \lesssim 0.5$.

Equations (77) and (82) give the initial conditions for the system

$$\begin{aligned}\frac{ds_3}{dx} &= -\frac{2\,\eta}{L}\int_{v_1(s_3,s_4)}^{v_2(s_3,s_4)} dv\,\frac{v(1-v)}{\sqrt{\mathcal{R}(v)}},\\ \frac{ds_4}{dx} &= \frac{\eta\,s_3}{L}\int_{v_1(s_3,s_4)}^{v_2(s_3,s_4)} dv\,\frac{1-v}{\sqrt{\mathcal{R}(v)}},\end{aligned} \tag{83}$$

where $v_i(s_3,s_4)$ $(i = 1,2,3)$ are determined as being the roots of the equation $\mathcal{R}(v,s_3,s_4) = 0$, where

$$\begin{aligned}\mathcal{R}(v,s_3,s_4) \equiv\ & v^3 - (M^2+2)v^2\\ &+\left[\left(\frac{M^2}{2} + 1\right)^2 - 4s_4\right]v - s_3^2.\end{aligned} \tag{84}$$

In Eqs. (83) L is also expressed in terms of the v's [see Eq. (76)].

In the present application of Whitham modulation theory it is important to notice that for fixed values of $\varkappa$, η, and M, the solution of Whitham equations depends on a single parameter $\bar{\rho}$ which is also a function of the same set of physical parameters ($\varkappa$, η, M) prescribed by the external potential and the boundary conditions of the Gross-Pitaevskii equation. Hence, the parameter $\bar{\rho}$ can be found from the condition that the solution of Whitham equations satisfies the correct boundary condition at $x \to -\infty$, namely that the envelopes of the density oscillations tend to the asymptotic value of the density:

$$v_1(x),\, v_2(x) \to 1 \quad \text{as} \quad x \to -\infty. \tag{85}$$

Some values of $\bar{\rho}$ calculated in this way are listed in the second row of Table I for $\eta = 0.05$, $M = 3$, and several values of $\varkappa$. We compare them with the values of $\bar{\rho}$ obtained by exact numerical solution of Eq. (46). As we see, the agreement is very good.

The $\varkappa$ dependence of $\bar{\rho} \equiv \rho(0)$ is shown in the right panel of Fig. 6 for several values of M. The η dependence of $\bar{\rho}$ is displayed in the left panel of the same figure for several values of $\varkappa$. This plot shows that $\bar{\rho}$ does not tend to unity in the limit $\eta \to 0$. This means that, in this limit, the flow pattern does not uniformly converge along the whole x axis to the exact solution found in Ref. 31 in the case $\eta \equiv 0$. Indeed, for the exact $\eta = 0$ solution, the downstream density is a constant [and then $\bar{\rho} = \rho(0) = \rho(+\infty) = 1$]. Rather, for small and finite η, the actual profile matches the exact $\eta = 0$ one in the large

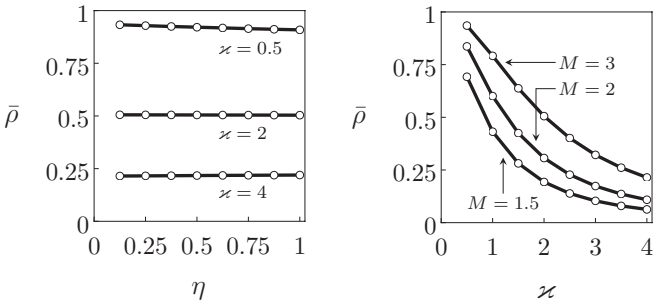

FIG. 6. $\bar{\rho} = \rho(0)$ as a function of η for $M = 3$ and different values of $\varkappa$ (left panel) and as a function of $\varkappa$ for $\eta = 0.05$ and several values of M (right panel).

region $-1/\eta \ll x \ll 1/\eta$ and then relaxes to the asymptotic density $[\rho(\pm\infty) = 1]$ at $|x| \gg 1/\eta$. This is confirmed by the numerical simulation performed in Sec. IV C.

A striking feature of the plot in the left panel of Fig. 6 is the extremely weak η dependence of $\bar{\rho}$. This important property of the theory can be explained by the simple fact that the space coordinate x and the parameter η enter into both the hydraulic approximation and Whitham equations only through the combination $\eta\, x$ [see Eqs. (51) and (83)]. As a result, η can be rescaled out of the exact relation (18) after averaging over fast oscillations in the dispersive shock region $x < 0$, so that we arrive to an equation which depends on η only through the small value of $\rho_x(0^+)$ [see Eqs. (79) and (82)]. If we neglect this term, then the resulting equation yields $\bar{\rho}$ as a function of M and $\varkappa$ only.

When $\bar{\rho}$ is found, all the parameters of the dispersive shock wave are determined, the functions $v_1(x)$, $v_2(x)$, $v_3(x)$ can be computed by solving Eqs. (83), and their substitution into Eqs. (75) yields the oscillatory structure upstream from the obstacle. The same value of $\bar{\rho}$ determines the hydraulic solution downstream from the obstacle. Thus, we reach a complete description of the nonlinear wave generated by a supercritical flow past a δ obstacle.

The accuracy of the theory is illustrated by Fig. 7. As we see, the agreement between the results of the combined Whitham and hydraulic approaches and the numerical computations is excellent. Note that Whitham method is perfectly valid in a regime where the perturbative theory of Sec. III seriously fails ($|\rho(x) - 1|$ is not small in Fig. 7). For illustrative reasons we have chosen a relatively large value of η ($\eta = 1$): We wanted to work in a regime where the overall modulations of the oscillating pattern occur over a characteristic length which is not too large with respect to the wavelength of the oscillations. As we see, even in this unfavorable case the agreement with the exact numerical results is very good.

The solution of the system (83) exists, and the upstream pattern can be described as a slowly modulated cnoidal wave, as long as its initial conditions can be found, that is, as long as the equation $\mathcal{R}(v, s_3(0), s_4(0)) = 0$ has three real roots. If η is strictly zero, then, choosing the normalization $\bar{\rho} = 1$ of Ref. 31, this equation reads

$$v^3 + (M^2 + 2)v^2 + (1 + 2M^2 + 4\varkappa^2)v - M^2 = 0. \quad (86)$$

Two of the roots coalesce and go into the complex plane when the discriminant of Eq. (86) vanishes. This corresponds to a

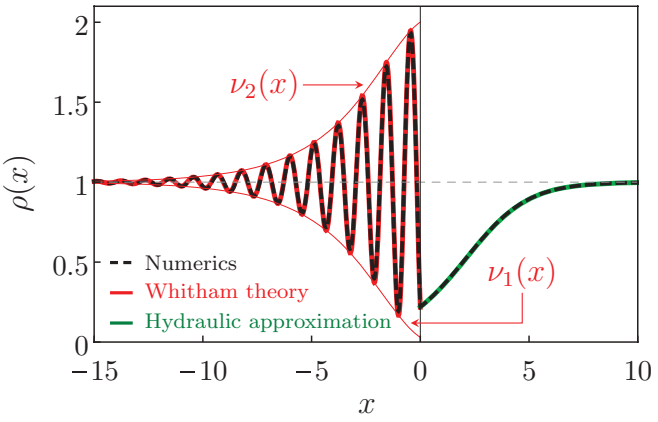

FIG. 7. (Color online) Comparison of the Whitham theory with the numerical solution of Eq. (46). The plot is drawn in the case $\eta = 1$, $M = 3$, and $\varkappa = 4$. The numerics corresponds to the dashed black line. Whitham envelopes are shown by thin red solid lines, and the upstream dispersive shock wave oscillatory structure obtained by substitution of the solution of the Whitham Eqs. (83) into Eqs. (75) is shown by a red solid line (for $x \leqslant 0$). The downstream ($x \geqslant 0$) hydraulic approximation is shown by a green solid line.

boundary between possible parameters in the plane $(\varkappa, M)$ determined by the condition

$$\varkappa_b^2 = \tfrac{1}{32}[M(M^2 + 8)^{3/2} + M^4 - 20M^2 - 8]. \quad (87)$$

The same boundary was already found in a different analytical form in Ref. 31 for a nondamped system. In our problem ($\eta \neq 0$, $\bar{\rho} \neq 1$), this boundary is changed and can be found by numerically determining when the discriminant of Eq. (84) vanishes. However, when $\eta \neq 0$, as we shall see in Sec. IV C, new stationary solutions appear when $\varkappa$ gets so large that the upstream flow is not described by a modulated cnoidal wave, making the determination of the domain of validity of Whitham approach less crucial than when $\eta = 0$.

C. Numerical results

In this section we present results of the full numerical solution of Eq. (46). We used a shooting method, starting the numerical integration from large and positive x with an initial behavior given by the prediction of perturbation theory. Typical results are displayed in Fig. 8.

The upper plots of this figure are drawn for $M = 3$ which is a velocity deep enough in the supersonic regime for Whitham theory of Sec. IV B to apply over a rather large range of values of $\varkappa$. The left plot of the upper row corresponds to $\varkappa = 0.5$. For this value of $\varkappa$, perturbation theory is valid upstream ($x < 0$) but fails for positive x, whereas the hydraulic approximation is quite accurate in this region, as shown by the dashed line in this plot. For $\varkappa = 4$ (right plot of the upper row of Fig. 8), the density profile shows the same features, but in this case perturbation theory seriously fails, whereas the downstream wave pattern being typical for a damped cnoidal wave is very well described by Whitham theory (not shown, because indistinguishable from the numerical result).

The two rows below the upper one correspond to $M = 1.2$ and $M = 1$. They are interesting because they show that, whereas perturbation theory fails in the absence of damping

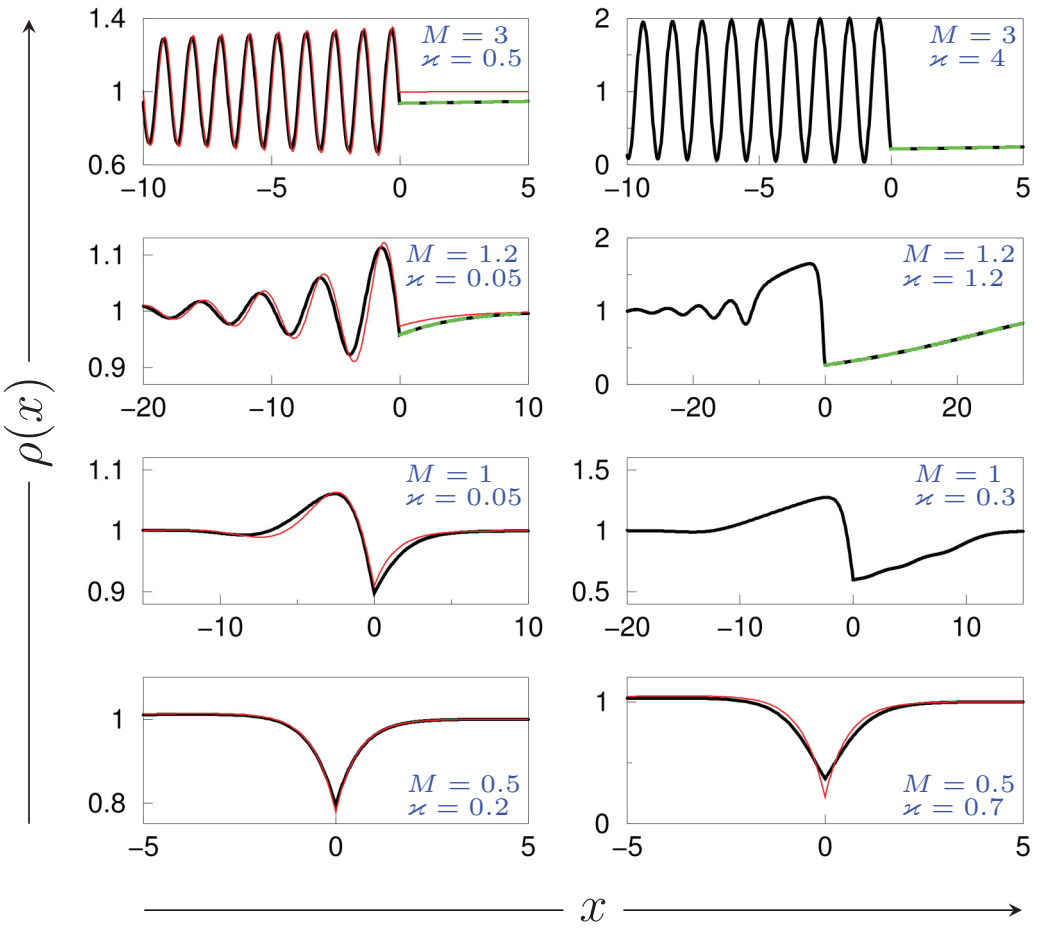

FIG. 8. (Color online) Different profiles $\rho(x)$ for flows past a δ-impurity potential of type (19). For all the profiles the damping parameter is $\eta = 0.05$. For the upper row $M = 3$, then $M = 1.2$ for the row below, $M = 1$ for the following one, and finally $M = 0.5$ for the lower row. The value of $\varkappa$ is indicated in each plot. In each plot the black solid line corresponds to the numerical solution of Eq. (46), the (red online) thin line to the perturbative result and the (green online) dashed line to the result of the hydraulic approximation which is only relevant for $x \geqslant 0$ (see Sec. IV A).

when $M \simeq 1$, for $\eta \neq 0$ it has a regime of validity even for velocities M close to unity. This is illustrated by the good agreement of the perturbative results with the numerics displayed in the two left plots of the central rows (which are both drawn in the case $\varkappa = 0.05$). It is also interesting to remark that for $M = 1$, no stationary solution exists when $\eta = 0$, whereas here we could find such solutions up to $\varkappa = 0.3$ (see the right plot of the third row). The values $M = 1$ and $\varkappa = 0.3$ are close to the boundary marking the end of the existence of stationary solutions when $\eta = 0.05$. In this case the downstream wave pattern shows small scale disturbances which were recognized in Ref. 35 as typically occurring near the end of the stationary regime.

The second upper row of Fig. 8 corresponds to $M = 1.2$. In this case, when $\eta = 0$, there is no stationary solution for $\varkappa \geqslant 0.0495$ [see Eq. (87) or Ref. 31]. As seen on the figure, when $\eta = 0.05$, one can find stationary solutions for much larger values of $\varkappa$ (up to $\varkappa \simeq 1.2$; see the corresponding plot). However, the density profile found in this case is very different from a damped cnoidal wave. It seems to be a stationary version of a type of time-dependent profiles studied in Ref. 50 for the case $\eta = 0$: A plateau develops just upstream from the obstacle which terminates when $x \to -\infty$ by a dispersive shock wave. Here, when $\eta \neq 0$, the plateau and the shock wave are damped because the specific form of the modified Gross-Pitaevskii Eq. (3) favors relaxation towards $\rho = 1$.

The lower row of Fig. 8 displays results corresponding to a subsonic obstacle ($M = 0.5$). For this value of the velocity, there is no stationary solution in the $\eta = 0$ case for $\varkappa \geqslant 0.59$.[31,51] As illustrated by the right plot of this row (drawn for $\varkappa = 0.7$) in the presence of damping, solutions exist for slightly larger values of $\varkappa$. However we find that, when η passes from 0 to 0.05, the range of values of $\varkappa$ allowing for a stationary solution does not increase in the subsonic case as much as it does in the supersonic region. This is illustrated by Fig. 9 where we represent the domain of existence of stationary flows in the $(\varkappa, M)$ plane. This domain corresponds to the shaded region in the figure and was numerically determined in the case $\eta = 0.05$. The large increase of the stationary domain for supersonic flows in the presence of damping is due to the occurrence, when $\eta \neq 0$, of a new class of profiles with an upstream plateau, as explained above and illustrated in the right plot of the second row from the left in Fig. 8 (corresponding to $M = 1.2$ and $\varkappa = 1.2$).

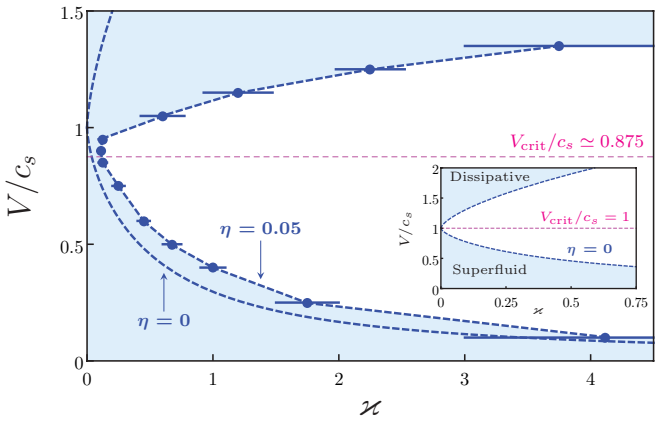

FIG. 9. (Color online) Different regimes of flow past a δ-impurity potential of type (19) in the $(\varkappa, M = V/c_s)$ plane. The main plot corresponds to the dissipative system (with $\eta = 0.05$). The inset is drawn for $\eta = 0$. In both plots the shaded regions correspond to stationary flows, the white ones to time-dependent and dissipative flows and the horizontal dashed line indicated the transition from a localized wake to a regime of Cherenkov emission as predicted by perturbation theory. In the inset, the subsonic ($M < 1$) shaded region is superfluid and the supersonic ($M > 1$) one is dissipative; the exact equation of the boundaries between the different domains is given in Ref. 31. In the main plot the dots with error bars represent the numerically determined boundary of the stationary domain. They are connected by a dashed line to guide the eye. The other dashed line in this plot represents the $\eta = 0$ result (shown for comparison).

This type of profile cannot be stationary with the boundary condition $\rho(x \to \pm\infty) = 1$ in a nondissipative system. Here, the damping term in Eq. (3) provides a mechanism allowing the downstream relaxation from $\rho(0) < 1$ to $\rho(x \to \infty) = 1$ and the upstream dispersive shock is stabilized by dissipation.

The inset in Fig. 9 represents the exact domain of stationary flows for $\eta = 0$, as analytically determined in Ref. 31. One can identify three regimes depending on the value of the parameters $\varkappa$ and $M = V/c_s$: (i) subsonic, stationary, and superfluid, (ii) dissipative and time dependent, (iii) dissipative, stationary, and supersonic. As seen in this inset, regimes (i) and (iii) are always separated by the time-dependent region (ii). This feature is also valid for a thick obstacle[37] and is in contradiction with the (wrong) prediction of perturbation theory for $\eta = 0$. Indeed, in the nondissipative case, perturbation theory always fails when V is close to c_s[31] and in this case the true flow gets time dependent. On the contrary, for finite $\eta \ll 1$ we showed in Sec. III that the perturbative prediction of existence of a stationary flow pattern *for all velocities* is valid until $\varkappa \sim \eta^{1/3}$. This is corroborated by the numerical results displayed in Fig. 9 for $\eta = 0.05$. In this case $\eta^{1/3} \simeq 0.3$ whereas the largest value of $\varkappa$ for which a stationary flow exists for all M is numerically found to be $\simeq 0.1$.

V. CONCLUSION

In the present work we have analyzed the flow of a one-dimensional polariton condensate in motion with respect to an obstacle in a situation of nonresonant pumping. We solved the problem perturbatively and showed that at this level there exists a smooth crossover from a viscous flow to a regime where the drag is mainly dominated by wave resistance. Perturbation theory predicts that this occurs at a velocity $M_{\rm crit}$ independent of the potential representing the obstacle. We argued that in the case of a δ impurity [represented by a potential of type (19)] the perturbative approach is valid *for all velocities* in the regime $\varkappa \times \max\{1, \eta^{-1/3}\} \ll 1$, where η is the dimensionless damping parameter defined in Eq. (2). As shown in the previous section this implies that stationary profiles indeed exist for all velocities if $\varkappa \lesssim \min\{1, \eta^{1/3}\}$. In this case there is a continuous transition from a dissipative drag to a regime dominated by the wave resistance.

However, from Fig. 9 we are led to refine this discussion of the transition between a regime where the wake is localized in the vicinity of the obstacle and a regime of (damped) Cherenkov radiation: We see on the example of the δ impurity that for a strong enough potential the two types of flows are separated by a time-dependent regime, as typically observed in BEC atomic vapors. In this case one cannot state that the crossover is smooth.

The comparison of our results with the ones of Ref. 29 leads to the conclusion that the gross features of the wave pattern discussed in the present work are quite independent of the technique used for setting the fluid into motion with respect to the obstacle. However, we use a specific model [Eq. (1)] with *nonresonant pumping* which is more relevant for the experiment presented in Ref. 9. In this experiment, a two-dimensional supersonic cloud of polaritons colliding with an obstacle was observed to induce a rather well defined wake, with oscillations having an apparently specified wavelength. The same feature was observed numerically in Ref. 26 (see also the discussion in Refs. 34 and 52). The perturbative results allow one to understand this phenomenon in a one-dimensional setting: The pattern of the upstream oscillatory wake in a supercritical flow ($V > V_{\rm crit}$) is governed by the complex wave vectors q_1 and q_2; see Sec. III. Also in the nonlinear approach (Whitham theory of Sec. IV B) does the wake keep a simple shape: Perturbation theory fails to properly account for the amplitude of the oscillations, but it still approximatively describes their wavelength.

An important result of our work is the demonstration that it is difficult to assess on the superfluidity of a polariton system just by studying the density perturbation past a localized obstacle. In particular, we showed that the absence of long-range wake cannot be used as a criterion for the absence of dissipation.

Finally, this work naturally calls for developments. One would first like to precisely determine the domain of time-dependent nonlinear flows in presence of damping. Secondly, one would like to extend the present work for taking into account polarization effects, and, thirdly, it is natural to apply the perturbative approach to higher dimensions. Works in these directions are in progress.

ACKNOWLEDGMENTS

We thank A. Amo, J. Bloch, M. Rabaud, and M. Richard for fruitful discussions. A.M.K. thanks LPTMS (Université Paris-Sud and CNRS), where this work was done, for kind hospitality. This work was supported by the project NLQUAFLU of RTRA Triangle de la Physique.

APPENDIX A: POLES OF THE RESPONSE FUNCTION $\chi(q, -Mq)$

In this Appendix we determine—as a function of M—the location in the complex q plane of the poles of the response function (13) evaluated at $\omega = -Mq$. Considering the expression of χ one sees that these poles are the three zeros of $D(q, -Mq)/q$. We denote them as q_1, q_2, and q_3. They are solutions of Eq. (21). This equation has three imaginary solutions when its discriminant $\Delta = 256(1-M^2)^3/27 - 64\,\eta^2 M^2$ is positive. The condition $\Delta > 0$ is equivalent to $M < M_{\rm crit}$ where the expression of $M_{\rm crit}$ is given in Eq. (26). In this case, defining

$$\theta = \arctan\left(\frac{8\eta M}{\sqrt{\Delta}}\right), \tag{A1}$$

one finds

$$\begin{aligned} q_1 &= 4i\sqrt{\frac{1-M^2}{3}}\sin\left(\frac{\theta}{3}-\frac{\pi}{3}\right),\\ q_2 &= -4i\sqrt{\frac{1-M^2}{3}}\sin\left(\frac{\theta}{3}\right),\\ q_3 &= 4i\sqrt{\frac{1-M^2}{3}}\sin\left(\frac{\theta}{3}+\frac{\pi}{3}\right). \end{aligned} \tag{A2}$$

Alternatively one can write $q_1 = i(-A+B)$, $q_2 = -2iB$, and $q_3 = i(A+B)$ with

$$\begin{bmatrix} A\\ B\end{bmatrix} = 2\sqrt{1-M^2}\begin{bmatrix}\cos(\theta/3)\\ \frac{1}{\sqrt{3}}\sin(\theta/3)\end{bmatrix}. \tag{A3}$$

If $\Delta < 0$ (i.e., if $M > M_{\rm crit}$), defining

$$D_{(\pm)} = \left(4\eta M \pm \tfrac{1}{2}|\Delta|^{1/2}\right)^{1/3}, \tag{A4}$$

one finds

$$\begin{aligned} q_1 &= D_{(+)}\exp(-i\pi/6) - D_{(-)}\exp(i\pi/6),\\ q_2 &= -D_{(+)}\exp(i\pi/6) + D_{(-)}\exp(-i\pi/6),\\ q_3 &= i(D_{(+)} + D_{(-)}). \end{aligned} \tag{A5}$$

Alternatively, one can write $q_1 = E - iF$, $q_2 = -E - iF$, and $q_3 = 2iF$ with

$$E = \frac{\sqrt{3}}{2}(D_{(+)} - D_{(-)}), \quad F = \frac{1}{2}(D_{(+)} + D_{(-)}). \tag{A6}$$

One can verify that $\sum_{\ell=1}^{3} q_\ell = 0$ for all values of M, as already clear from the form of Eq. (21). A similar relation holds for the residues of $\chi(q, -Mq)$ whose expressions are given in Eq. (23): $\sum_{\ell=1}^{3} {\rm Res}(q_\ell) = 0$.

The typical M dependence of the position of the poles in the complex plane is illustrated in Fig. 10. When $M = 0$ one has $\theta = 0$, $q_2 = 0$, and $q_3 = -q_1 = 2i$. When M is increased from zero, q_1 and q_2 get closer on the imaginary axis until they collide (when $M = M_{\rm crit}$) and then acquire a finite real part. When $M \to \infty$, $q_3 \to i\,0^+$, and $q_{(1,2)} \to (+,-)\infty - i\,0^+$. A similar behavior has already been found in Refs. 26 and 34.

A useful approximation for the expression of the poles is obtained when $\eta M/|M^2-1|^{3/2} \ll 1$. In this case one obtains,

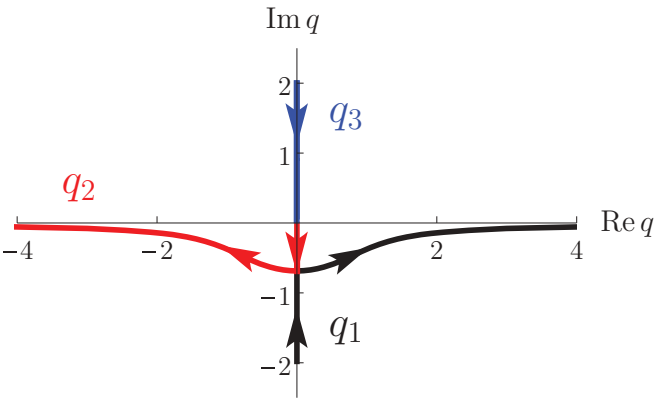

FIG. 10. (Color online) Position of q_1, q_2, and q_3 in the complex q plane. The figure is drawn in the case $\eta = 0.1$. The arrows indicate the direction of motion of the poles when M increases from 0 to ∞[53].

when $M < M_{\rm crit}$,

$$\begin{aligned} q_{(1,3)} &\simeq i\left[(-,+)2\sqrt{1-M^2} + \frac{\eta M}{1-M^2}\right],\\ q_2 &\simeq -2i\,\frac{\eta M}{1-M^2}, \end{aligned} \tag{A7}$$

and when $M > M_{\rm crit}$,

$$\begin{aligned} q_{(1,2)} &\simeq (+,-)2\sqrt{M^2-1} - i\,\frac{\eta M}{M^2-1},\\ q_3 &\simeq 2i\,\frac{\eta M}{M^2-1}. \end{aligned} \tag{A8}$$

The above expressions are valid up to corrections of relative order $\eta^2 M^2/|M^2-1|^3$. It is interesting to notice that expansions (A7) and (A8) are equally valid at large velocity and at small damping. Indeed, as discussed at the end of Sec. III D, at large velocity the effects of damping are negligible.

From the explicit expressions (A2) and (A5) of the q_ℓ's it is a simple matter to evaluate the integral (16) which permits one to compute the function $K(X)$. One gets

$$\begin{aligned} K(X \geqslant 0) &= i\,{\rm Res}(q_3)\,e^{iq_3X},\\ K(X \leqslant 0) &= -i[{\rm Res}(q_1)\,e^{iq_1X} + {\rm Res}(q_2)\,e^{iq_2X}]. \end{aligned} \tag{A9}$$

Formulas (A9) are valid for all M, but the explicit expressions for the q_ℓ's depend on M. For instance, when $M < M_{\rm crit}$ the q_ℓ's are all imaginary and K tends rapidly to zero when $|X| \to \infty$. On the other hand, when $M > M_{\rm crit}$ the exponential decrease of $K(X)$ gets weaker (because the imaginary part of the q_ℓ's is smaller) and $K(X \leqslant 0)$ oscillates (because q_1 and q_2 acquire a real part). The typical density perturbations associated with K [i.e., for a δ-peak potential of the form (19)] are sketched in the insets of Fig. 2. Note that the value of the q_ℓ's does not depend on η when $M = 0$ [i.e., within the theoretical description corresponding to Eq. (1)], the density perturbation induced by a motionless obstacle does not depend on the damping.

The expressions (A9) are equally valid in the absence of damping (i.e., when $\eta = 0$). In this case $M_{\rm crit} = 1$, $q_2 = 0$, and $q_3 = -q_1$ for $M < M_{\rm crit}$ and for $M > M_{\rm crit}$, $q_3 = 0$ whereas q_1 and q_2 are real and opposite [cf. Eqs. (A7) and (A8)]: For $M > M_{\rm crit}$ and $\eta = 0$ one observes undamped Cherenkov radiations ahead of the obstacle as discussed in the main text. For

$M > M_{\rm crit}$ and $\eta \neq 0$ these Cherenkov radiations are damped since in this case q_1 and q_2 have a nonzero imaginary part.

Finally, we need to evaluate the order of magnitude of the quantity $\varkappa |K(0)|$ at $M = M_{\rm crit}$ since, as argued in the main text (Sec. III B), this is the small parameter of perturbation theory for a δ-impurity obstacle. For $M = M_{\rm crit}$ one gets $\theta = \pi/2$, $q_1 = q_2 = -q_3/2 = -2i\sqrt{(1 - M_{\rm crit}^2)/3}$ [cf. Eqs. (A2)] and this yields

$$\varkappa K(0) = \frac{i\,\varkappa\sqrt{3}}{\sqrt{1 - M_{\rm crit}^2}} \quad \text{when} \quad M = M_{\rm crit}. \tag{A10}$$

From the expression (26) for $M_{\rm crit}$ one sees that $(1 - M_{\rm crit}^2)^{-1/2} \simeq \frac{1}{\sqrt{3}}(2/\eta)^{1/3}$ when $\eta \ll 1$ and tends to unity at large η, from which one obtains the estimate (27).

APPENDIX B: DERIVATION OF PERTURBED WHITHAM EQUATIONS

The general method of derivation of the Whitham equations for perturbed integrable equations which in their nonperturbed form belong to the Ablowitz-Kaup-Newell-Segur scheme was developed in Ref. 54 and it can be formulated as follows. Let the evolution equations of some field variables u_k have the form

$$\frac{\partial u_k}{\partial t} = K_k\left(u_m, \varepsilon\frac{\partial u_m}{\partial x}, \varepsilon^2\frac{\partial^2 u_m}{\partial x^2}, \dots\right) + R_k\left(u_m, \varepsilon\frac{\partial u_m}{\partial x}, \varepsilon^2\frac{\partial^2 u_m}{\partial x^2}, \dots\right), \tag{B1}$$

where a small parameter $\varepsilon \ll 1$ is introduced which measures the dispersion effects. It is supposed that a nonperturbed system,

$$\varepsilon\frac{\partial u_k}{\partial t} = K_k\left(u_m, \varepsilon\frac{\partial u_m}{\partial x}, \varepsilon^2\frac{\partial^2 u_m}{\partial x^2}, \dots\right), \tag{B2}$$

can be represented as a compatibility condition of two linear equations,

$$\begin{aligned} \varepsilon^2\chi_{xx} &= \mathcal{A}\chi, \\ \chi_t &= -\tfrac{1}{2}\mathcal{B}_x\chi + \mathcal{B}\chi_x, \end{aligned} \tag{B3}$$

where $\mathcal{A}$ and $\mathcal{B}$ depend on the u_k's, their space derivatives, and on the spectral parameter λ. It is assumed that the system (B2) has a periodic solution with wavelength $L \propto \varepsilon$ and it is parametrized by the constant parameters λ_i which appear in the finite-gap integration method in the following way. The second-order linear equations (B3) has two basis solutions $\chi_\pm$ and their product $g = \chi_+\chi_-$ satisfies a third-order differential equation which can be integrated once to give

$$\frac{\varepsilon^2}{2}gg_{xx} - \frac{\varepsilon^2}{4}g_x^2 - \mathcal{A}g^2 = \sigma P(\lambda), \tag{B4}$$

where σ is determined by the sign of the highest order term in $\mathcal{A}$ as a function of λ (i.e., $\mathcal{A} \sim -\sigma\lambda^r$ as $\lambda \to \infty$). Periodic solutions are distinguished by the condition that $P(\lambda)$ is a polynomial in λ and then λ_i are its zeros. We shall confine ourselves to the one-phase periodic solutions which physical variables depend on a single variable $x - V_\varphi t$ only.

In a modulated wave the parameters λ_i become slow functions of x and t whose evolution is described by the Whitham equations which in the case of (B1) and (B3) can be written in the form

$$\begin{aligned} &\frac{\partial\lambda_i}{\partial t} - \frac{\langle\mathcal{B}/g\rangle}{\langle 1/g\rangle}\frac{\partial\lambda_i}{\partial x} \\ &\quad= \lim_{\varepsilon\to 0}\left\{\frac{\sigma}{\langle 1/g\rangle\prod_{m\neq i}(\lambda_i - \lambda_m)}\right. \\ &\qquad\left.\times\sum_k\left\langle\left(\frac{\partial\mathcal{A}}{\partial u_k}R_k + \dots + \frac{\partial\mathcal{A}}{\partial u_k^{(\ell_k)}}\frac{\partial^{(\ell_k)}R_k}{\partial x^{(\ell_k)}}\right)g\right\rangle\right\}, \end{aligned} \tag{B5}$$

where ℓ_k denotes the highest order of derivative of u_k entering in $\mathcal{A}$. The angle brackets denote the averaging over one wavelength:

$$\langle\mathcal{F}\rangle = \frac{1}{L}\int_0^L dx\,\mathcal{F}. \tag{B6}$$

The spectral parameter λ should be put equal to λ_i after averaging.

We shall apply here this scheme to the perturbed nonlinear Schrödinger (NLS) equation,

$$i\varepsilon\,\psi_t + \tfrac{1}{2}\varepsilon^2\psi_{xx} - |\psi|^2\psi = iG(|\psi|^2)\psi, \tag{B7}$$

where $G(\rho)$ is a real function of the density $\rho = |\psi|^2$. Equation (3) pertains to this type [with $G(\rho) = \eta(1 - \rho)$]. In the case of Eq. (B7) we have two field variables ψ, ψ^*, and, correspondingly, two terms of perturbation in Eq. (B1):

$$R_\psi = G(\rho)\psi/\varepsilon, \quad R_{\psi^*} = G(\rho)\psi^*/\varepsilon. \tag{B8}$$

For nonperturbed NLS equation the linear system (B3) is specified as

$$\mathcal{A} = -\lambda^2 - i\varepsilon\lambda\frac{\psi_x}{\psi} + \psi^*\psi - \frac{\varepsilon^2}{2}\frac{\psi_{xx}}{\psi} + \frac{3\varepsilon^2}{4}\frac{\psi_x^2}{\psi^2}, \tag{B9}$$

$$\mathcal{B} = -\lambda + \frac{i\varepsilon}{2}\frac{\psi_x}{\psi}. \tag{B10}$$

Substitution of (B9) and (B10) into (B5) shows that, in the expression to be averaged [in the right-hand side of (B5)], the leading term in powers of ε is equal to $2\langle G\rho g\rangle/\varepsilon$. The averaging can be performed with the use of equations known from the theory of periodic solutions of the NLS equation (see, e.g., Ref. 49):

$$\begin{aligned} g &= \lambda - \mu_a, \quad \varepsilon\frac{d\mu_a}{dx} = 2\sqrt{-P(\mu_a)}, \\ -\frac{i\varepsilon}{2}\frac{\psi_x}{\psi} &= \frac{s_1}{2} - \mu_a, \qquad V_\varphi = \frac{s_1}{2}, \\ L &= \varepsilon\oint\frac{d\mu_a}{2\sqrt{-P(\mu_a)}}, \end{aligned} \tag{B11}$$

where $P(\mu_a) = \prod_i(\mu_a - \lambda_i)$ and $s_1 = \sum_i\lambda_i$. The quantity μ_a is known as the auxiliary eigenvalue in the finite-gap integration method. Hence, we obtain

$$\left\langle\frac{1}{g}\right\rangle = \left\langle\frac{1}{\lambda - \mu_a}\right\rangle = -\frac{2}{L}\frac{\partial L}{\partial\lambda_i}, \quad \left\langle\frac{\mathcal{B}}{g}\right\rangle = -1 + \frac{s_1}{L}\frac{\partial L}{\partial\lambda_i}. \tag{B12}$$

For calculating $\langle G\rho g\rangle$ we also take into account that μ_a can be expressed as a function of ρ in the following way (see Ref. 49):

$$\mu_a(\rho) = \frac{s_1}{4} + \frac{-j + i\sqrt{\mathcal{R}(\rho)}}{2\rho}, \tag{B13}$$

where

$$\mathcal{R}(\nu) = (\nu - \nu_1)(\nu - \nu_2)(\nu - \nu_3), \quad j^2 = \nu_1\nu_2\nu_3, \tag{B14}$$

$$\begin{aligned} \nu_1 &= \tfrac{1}{4}(\lambda_1 - \lambda_2 - \lambda_3 + \lambda_4)^2, \\ \nu_2 &= \tfrac{1}{4}(\lambda_1 - \lambda_2 + \lambda_3 - \lambda_4)^2, \\ \nu_3 &= \tfrac{1}{4}(\lambda_1 + \lambda_2 - \lambda_3 - \lambda_4)^2, \end{aligned} \tag{B15}$$

and

$$\varepsilon \frac{d\rho}{dx} = 2\sqrt{\mathcal{R}}. \tag{B16}$$

Then we obtain the Whitham equations for the Riemann invariants λ_i in the form,

$$\frac{\partial \lambda_i}{\partial t} + v_i \frac{\partial \lambda_i}{\partial x} = -\frac{v_i - s_1/2}{\prod_{m\neq i}(\lambda_i - \lambda_m)} \times \frac{2}{L}\int_{\nu_1}^{\nu_2} d\nu \, \frac{G(\nu)[(\lambda_i - s_1/4)\nu + j/2]}{\sqrt{\mathcal{R}(\nu)}}, \tag{B17}$$

with

$$v_i = \frac{s_1}{2} + \left(\frac{2}{L}\frac{\partial L}{\partial \lambda_i}\right)^{-1}, \quad i \in \{1,2,3,4\}. \tag{B18}$$

In the stationary case (i.e., when $\partial\lambda_i/\partial t = 0$ and $s_1 = 2\,V_\varphi = 0$), the Whitham equations simplify to

$$\frac{d\lambda_i}{dx} = \frac{2}{L}\frac{G_1\lambda_i + G_2}{\prod_{m\neq i}(\lambda_i - \lambda_m)}, \tag{B19}$$

where

$$\begin{aligned} G_1 &= -\int_{\nu_1}^{\nu_2} d\nu \, \frac{\nu\, G(\nu)}{\sqrt{\mathcal{R}(\nu)}}, \\ G_2 &= -\frac{j}{2}\int_{\nu_1}^{\nu_2} d\nu \, \frac{G(\nu)}{\sqrt{\mathcal{R}(\nu)}}. \end{aligned} \tag{B20}$$

For $G(\rho) = \eta(1 - \rho)$ we arrive at Eqs. (61) and (62).

[1] D. R. Allum, P. V. E. McClintock, A. Phillips, and R. W. Bowley, Philos. Trans. R. Soc. London A **284**, 179 (1977).

[2] O. Avenel and E. Varoquaux, Phys. Rev. Lett. **55**, 2704 (1985).

[3] C. A. M. Castelijns, K. F. Coates, A. M. Guénault, S. G. Mussett, and G. R. Pickett, Phys. Rev. Lett. **56**, 69 (1986).

[4] C. Raman, M. Kohl, R. Onofrio, D. S. Durfee, C. E. Kuklewicz, Z. Hadzibabic, and W. Ketterle, Phys. Rev. Lett. **83**, 2502 (1999).

[5] R. Onofrio, C. Raman, J. M. Vogels, J. R. Abo-Shaeer, A. P. Chikkatur, and W. Ketterle, Phys. Rev. Lett. **85**, 2228 (2000).

[6] D. E. Miller, J. K. Chin, C. A. Stan, Y. Liu, W. Setiawan, C. Sanner, and W. Ketterle, Phys. Rev. lett. **99**, 070402 (2007).

[7] P. Engels and C. Atherton, Phys. Rev. Lett. **99**, 160405 (2007).

[8] D. Dries, S. E. Pollack, J. M. Hitchcock, and R. G. Hulet, Phys. Rev. A **82**, 033603 (2010).

[9] A. Amo *et al.*, Nature (London) **457**, 291 (2009).

[10] A. Amo *et al.*, Nat. Phys. **5**, 805 (2009).

[11] G. Nardin *et al.*, Nat. Phys. **7**, 635 (2011).

[12] A. Amo *et al.*, Science **332**, 1167 (2011).

[13] D. Sanvitto *et al.*, Nat. Phot. **5**, 610 (2011).

[14] L. D. Landau, J. Phys. (USSR) **5**, 71 (1940); **11**, 91 (1947); Reprinted by I. M. Khalatnikov, in *An Introduction to the Theory of Superfluidity* (Perseus Publishing, Cambridge, 2000).

[15] In many instances the actual value of $V_{\rm crit}$ is lower than Landau's expectation. As Feynman first suggested [in *Progress in Low Temperature Physics*, Vol. I, edited by C. J. Gorter (North-Holland, Amsterdam, 1955), p. 17] this is linked to the emission of nonlinear perturbations and not of elementary excitations as implied by Landau criterion which is intrinsically perturbative.

[16] J. Kasprzak *et al.*, Nature (London) **443**, 409 (2006).

[17] D. Bajoni, P. Senellart, E. Wertz, I. Sagnes, A. Miard, A. Lemaitre, and J. Bloch, Phys. Rev. Lett. **100**, 047401 (2008).

[18] S. Utsunomiya *et al.*, Nat. Phys. **4**, 700 (2008).

[19] E. Wertz *et al.*, Nat. Phot. **6**, 860 (2010).

[20] L. Ferrier, E. Wertz, R. Johne, D. D. Solnyshkov, P. Senellart, I. Sagnes, A. Lemaitre, G. Malpuech, and J. Bloch, Phys. Rev. Lett. **106**, 126401 (2011).

[21] G. Grosso, G. Nardin, F. Morier-Genoud, Y. Léger, and B. Deveaud-Plédran, Phys. Rev. Lett. **107**, 245301 (2011).

[22] M. Wouters and I. Carusotto, Phys. Rev. Lett. **99**, 140402 (2007).

[23] J. Keeling and N. G. Berloff, Phys. Rev. Lett. **100**, 250401 (2008).

[24] T. C. H. Liew, A. V. Kavokin, and I. A. Shelykh, Phys. Rev. Lett. **101**, 016402 (2008).

[25] M. Wouters, Phys. Rev. B **77**, 121302(R) (2008).

[26] M. Wouters and I. Carusotto, Phys. Rev. Lett. **105**, 020602 (2010).

[27] More satisfactory recent microscopic accounts of dissipative effects are given in I. G. Savenko, E. B. Magnusson, and I. A. Shelykh, Phys. Rev. B **83**, 165316 (2011); and in M. H. Szymanska, J. Keeling, P. B. Littlewood, arXiv:1206.1784.

[28] P.-É. Larré, N. Pavloff, and A. Kamchatnov (unpublished).

[29] A. Berceanu, E. Cancellieri, and F. M. Marchetti, J. Phys.: Condens. Matter **24**, 235802 (2012).

[30] D. L. Kovrizhin and L. A. Maksimov, Phys. Lett. A **282**, 421 (2001).

[31] P. Leboeuf and N. Pavloff, Phys. Rev. A **64**, 033602 (2001).

[32] N. Pavloff, Phys. Rev. A **66**, 013610 (2002).

[33] G. E. Astrakharchik and L. P. Pitaevskii, Phys. Rev. A **70**, 013608 (2004).

[34] M. Wouters and I. Carusotto, Superlattice. Microst. **43**, 524 (2008).

[35] A. M. Kamchatnov and Y. V. Kartashov, Europhys. Lett. **97**, 10006 (2012).

[36] We use the convenient denomination "speed of sound" for c_s although very long-wavelength modes do not propagate in the presence of damping and thus the sound velocity is only properly defined in the absence of damping [see, however, the remark after Eq. (11) in Sec. III A].

[37] A. M. Leszczyszyn, G. A. El, Yu. G. Gladush, and A. M. Kamchatnov, Phys. Rev. A **79**, 063608 (2009).

[38] It is interesting to note that nonlinear effects cannot be neglected either in capillary-gravity waves near the threshold for emission of the Kelvin wake; see, e.g., F. Dias and C. Kharif, Annu. Rev. Fluid Mech. **31**, 301 (1999).

[39]T. Burghelea and V. Steinberg, Phys. Rev. Lett. **86**, 2557 (2001).
[40]J. Browaeys, J.-C. Bacri, R. Perzynski, and M. I. Shliomis, Europhys. Lett. **53**, 209 (2001).
[41]E. Raphaël and P.-G. de Gennes, Phys. Rev. E **53**, 3448 (1996).
[42]M. Le Merrer, C. Clanet, D. Quéré, E. Raphaël, and F. Chevy, Proc. Natl. Acad. Sci. USA **108**, 15064 (2011).
[43]As discussed in the paragraph below Eq. (45), the drag force is even totally dominated by the wave resistance when $M \to \infty$.
[44]This is because $\hat{f}_{\rm ext}(q_M \to \infty) = 0$. Roughly speaking, this means that the wave drag is negligible when the de Broglie wavelength $\hbar/(mV)$ gets smaller than the typical size of the potential.
[45]M. Albert, T. Paul, N. Pavloff, and P. Leboeuf, Phys. Rev. Lett. **100**, 250405 (2008).
[46]T. Paul, M. Albert, P. Schlagheck, P. Leboeuf, and N. Pavloff, Phys. Rev. A **80**, 033615 (2009).
[47]Note that the hydraulic approximation is also valid for describing the long-distance upstream wake in the subsonic case.[35]
[48]G. B. Whitham, *Linear and Nonlinear Waves* (Wiley–Interscience, New York, 1974).
[49]A. M. Kamchatnov, *Nonlinear Periodic Waves and Their Modulations—An Introductory Course* (World Scientific, Singapore, 2000).
[50]A. M. Kamchatnov and N. Pavloff, Phys. Rev. A **85**, 033603 (2012).
[51]V. Hakim, Phys. Rev. E **55**, 2835 (1997).
[52]I. Carusotto and C. Ciuti, Rev. Mod. Phys. (to be published), arXiv:1205.6500.
[53]Note that q_3 initially slightly increases above $2i$ when $M \simeq 0$ [cf. Eqs. (A7)]. For legibility this small feature is not accounted for by the direction of the red arrow in Fig. 10.
[54]A. M. Kamchatnov, Physica D **188**, 247 (2004).